universität wien

# MASTERARBEIT

Titel der Masterarbeit

## Studies of a triple GEM detector setup


verfasst von

Achim Franke, BSc


angestrebter akademischer Grad

Master of Science (MSc)

Wien, 2015

| | |
|---|---|
| Studienkennzahl lt. Studienblatt: | A 066 876 |
| Studienrichtung lt. Studienblatt: | Masterstudium Physik UG2002 |
| Betreut von: | Dr. Johann Zmeskal, Privatdozent |

# Abstract

The main goal of this thesis is to study the stable operation of a triple-GEM detector with pure gases. Therefore, as a first step, we had to perform several improvements on the already existing detector. These improvements include new shielding of the preamplifier electronics, a different anode as new readout structure and a better mounting device for the radioactive source. We also had to build a data acquisition system (DAQ) based on NIM and CAMAC standards which allows to analyze events coming from the detector. After completing these preparations, first measurements with an $ArCO_2$ gas mixture and a $^{137}$Cs-source were done along single channels to test the stability of the GEM-detector over time as well as to find the optimal voltage in between the GEM foils. The next step was to improve the setup to allow for multichannel measurements. This is important for comparing different channels with each other directly to find out possible crosstalk and signal splitting between channels as well as differences in amplification.

To determine the gain of the triple-GEM detector, one measurement with a $^{55}$Fe-source was performed, giving a total gain of about 10,000 for our normally used voltage-settings over all 3 GEM-foils. After that we started measuring pure gases, beginning with the noble gases argon and neon, both of which could be measured successfully under different conditions (pressure, voltage).

As a final step, a first measurement with pure hydrogen in a triple-GEM detector could be realized. We were able to work with a high voltage difference of over 450 V in between each GEM and could thereby collect data from this pure hydrogen measurement over a time of 2.5 hours. A slightly lower gain as in $ArCO_2$ under stable conditions was reached, leading to a total of over 369,000 events in 4 channels. The measurement data set represents a valuable input for further design studies to build an active target GEM-TPC.

# Zusammenfassung

Das Hauptziel dieser Masterarbeit ist der stabile Betrieb eines dreifach-GEM Detektors mit Reingasen. Dazu führten wir einige Verbesserungen an einem bereits vorhandenen Detektor durch. Diese Verbesserungen beinhalten unter anderem eine neue Abschirmung der Vorverstärkerelektronik, eine neue Auslesestruktur in Form einer Anode bestehend aus Pixeln sowie eine Haltevorrichtung für die radioaktive Quelle. Desweiteren wurde ein neues Datenerfassungssystem basierend auf dem NIM und CAMAC-Standard zur Analyse der gemessenen Ereignisse aufgebaut. Nach Abschluss dieser Vorbereitungen wurden Messungen mit $ArCO_2$ Gas und einer $^{137}$Cs-Quelle von einzelnen Kanälen durchgeführt, um sowohl die zeitliche Stabilität des Detektors zu testen als auch die optimale Spannung zwischen einzelnen GEM-Folien zu finden. Anschließend konnte der Aufbau soweit verbessert werden, dass bis zu 4 Kanäle gleichzeitig messbar sind. Damit ist es möglich, verschiedene Kanäle zu vergleichen und ein eventuelles Übersprechen zwischen einzelnen Kanälen bzw. die Aufteilung des Signals auf benachbarte Pixel zu testen sowie Unterschiede in der Verstärkung einzelner Kanäle herauszufinden. Zur Bestimmung der Gasverstärkung unseres dreifach-GEM Detektors wurde eine Messung mit einer $^{55}$Fe-Quelle durchgeführt. Dies ergab eine Gasvervielfachung von etwa 10,000 über alle 3 GEM-Folien bei unseren üblicherweise genutzten Spannungseinstellungen. Anschließend wurden Messungen mit Reingasen gestartet, beginnend mit Argon und Neon, die beide erfolgreich unter verschiedenen Bedingungen gemessen werden konnten.
Als letzten Schritt war es uns möglich, eine erste Messung mit reinem Wasserstoff in einem dreifach-GEM Detektor zu realisieren. Wir konnten erfolgreich eine Spannungsdifferenz von über 450 V zwischen einzelnen GEM-Folien anlegen und damit Daten mit reinem Wasserstoff aufnehmen. Wir konnten in einer 2,5-stündigen Messung einen Verstärkungsfaktor leicht unterhalb dem für $ArCO_2$ unter stabilen Bedingungen erreichen, wobei eine Gesamtzahl von über 369.000 Events in 4 Kanälen gemessen wurde. Die gemessenen Daten liefern einen wertvollen Beitrag für zukünftige Designstudien zum Bau einer aktiven "Target-TPC" mit GEM-Auslese.

# Acknowledgements

First and foremost I would like to express my gratitude to my supervisor Dr. Johann Zmeskal for his continued support and his useful tips and help with my ongoing questions throughout this master thesis. I also want to thank him for his patience in answering my emails and editing this thesis.
Furthermore I would like to thank Ing. Herbert Schneider for his help in solving several technical problems throughout my time working on this thesis.
For his support with software problems and programming questions I want to thank Dr. Michael Cargnelli.
I am grateful to Leopold Stohwasser, Ing. Doris Stückler and Mark Pruckner for all technical assistance.
I also want to thank Prof. Eberhard Widmann and the whole team at the Stefan Meyer Institute for giving me the opportunity to realize this master thesis.
Thanks goes to Dražen Vrzan, who has given me his precious critique and proofreading.
My gratitude goes to my parents and my whole family, without whose mental and financial support I would not have been able to achieve my goals.
Last but not least, I want to thank my girlfriend, Stella Bevilaqua, for all her love and support during the time of writing this thesis.

# List of Figures

# Contents

# 1. Introduction

## 1.1. Setup - Statement of the problem

This master thesis is about the performance study of a particle detector consisting of 3 gas electron multiplier foils (GEM). To do that, a first step is to produce the GEM foils and an appropriate device to install them. This test chamber needs to be vacuum sealed to prevent penetration of external gases like oxygen or $H_2O$.
After setting up the detector it is necessary to build a signal path to process data coming from the detector readout. This includes several amplifiers: A preamplifier, a shaping amplifier in the second part of our measurement and a main amplifier, and finally a single- or multichannel-analyzer with integrated analog-to-digital converter (ADC) to convert the pulse height of the signal to a numerical value and a way to process the data in a computer. For the measuring-process it is important to ensure a controlled operation of the detector under different conditions including several gas mixtures, pressures and operation voltages and to ensure to work with a clean chamber gas with small impurities.
To start with, single channels are measured one by one to compare them with each other and test for variations in the gain between different channels under stable operation. Later on multichannel measurements are performed, 4 channels can be compared to each other within a measurement period. This will be done at first with a mixed gas ($ArCO_2$) which is then exchanged with several pure gases including argon, neon and hydrogen. These gases will be tested under different conditions. Not many experiments with GEM-detectors using pure gases, especially hydrogen, have been realized up to the present day.

## 1.2. Research Objectives

The main goal of this thesis is to study the operation of the triple-GEM detector with pure gases, which is essential for future detector development. Therefore, it is necessary to perform several experiments with pure gases and be able to reproduce the outcome in different test runs. Once the behavior of the GEMs under different conditions is studied, important input will be delivered for the design of an active target GEM-TPC, as is currently planned for the AMADEUS experiment at the DA$\Phi$NE-collider at the INFN Frascati National Laboratory in Frascati, Italy [1].

In this work, we concentrate on measurements (gain and stability tests) to operate the triple-GEM with pure gases under a voltage condition where it is possible to produce the necessary charge to detect events through the readout structure. Once that is the case, the gain of the 3 GEMs can be calculated and compared for measurement runs with different gases and under different voltage conditions.
The steps to achieve that goal have already been outlined in sec. 1.1 and will now be explained in more detail:
In our setup we have a 16x16=256 channel pixel-readout, each of which can be measured separately. Out of that, we are using a 4x4 matrix. As a first test, each channel is measured on its own over several hours, generating a pulse-height histogram. To check the reliability of the detector over a certain amount of time, measurements in different runs will be compared.
After completing these tests, an upgrade was installed to enable multichannel measurements, allowing to measure 4 channels at once. A detailed description follows in chapter 4.1.3, see also figure 4.13. Using this 4 channel setup it is possible to determine charge splitting between neighboring channels and to check for stable gain conditions. Once several channel-combinations are tested and analyzed, the gas in the detector is changed from an $ArCO_2$-mixture to different pure gases like argon, neon and hydrogen. Each of these gases is then measured in one of the channel-combinations to study the gas-amplification for a given voltage setting.
To determine the gas amplification in the GEM-detector, another measurement is performed with a $^{55}$Fe-source with emission of about 6 keV X-rays. With all these measurements, we will have a basic data set for the design of an active target GEM-TPC.

# 2. Physical Principles

## 2.1. Particle Detectors

In experimental particle physics as well as nuclear physics, a particle detector is a device to detect and/or track different particles. Depending on the kind of particle one wants to detect, there is a wide variety of different particle detectors, each with its own assets and drawbacks. Many modern detector systems can also be used to measure properties of the particles like spin, charge or momentum. The large variety of different detectors includes ionization chambers, proportional counters, scintillation detectors, semiconductor detectors and other types.
Since the main focus of this work is on a gaseous detector type called "Gas Electron Multiplier" (GEM), I will not go over other detector types in detail. For further information about these see [2].

Particle detector systems are used in many collider experiments, for example:

- At CERN:
  - LHC: CMS, ATLAS, ALICE
  - SPS: COMPASS
- KLOE-experiment at the DA$\Phi$NE-collider at the INFN LNF

Each of these experiments consists of different detectors, e.g. the detector-system used in CMS consists of a silicon tracker close to the interaction region, surrounded by a scintillating crystal electromagnetic calorimeter, which itself is surrounded by a hadronic calorimeter and 3 different muon detectors [3]. ALICE uses a large TPC and in future with GEM readout [4], KLOE has a large drift chamber as tracking detector [5]. One of the first experiments using GEMs was the COMPASS experiment at the SPS at CERN [6], which started collecting data in 2002.

## 2.2. Gas Electron Multiplier

A Gas Electron Multiplier (GEM) is a detector based on gaseous ionization, which was invented by Fabio Sauli in 1996 [7]. The GEM principle is as follows: Electrons are guided to the GEM foils via an electric field and then amplified within the hole, because of the huge electric field generated there. There several thousand electrons per incident particle can be produced. A GEM consists of an insulating Kapton-foil, which is coated with copper on both sides and has small holes pierced through it. An example is shown in figures 2.1 and 2.2.

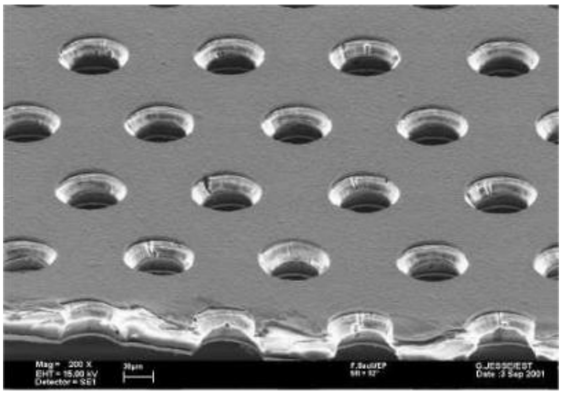

**Figure 2.1.:** GEM under microscope [8]

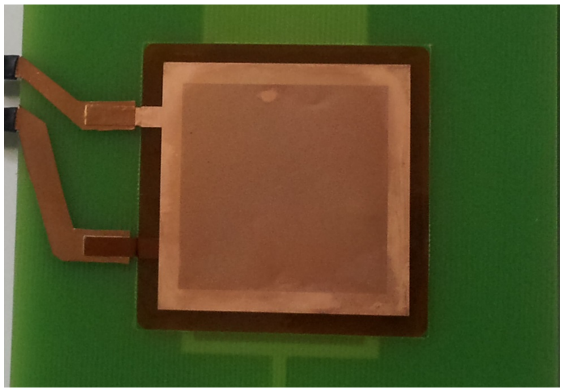

**Figure 2.2.:** GEM foil glued on frame

To achieve the desired gas amplification, a voltage of about 300. . . 400 V is applied between the top and bottom side of the GEM foil. Each foil has a thickness of 50 $\mu$m, so a high electric field strength of 60. . . 80 kV/cm can be reached. The holes have a conical shape with an outer diameter of 80 $\mu$m, an inner diameter of 50 $\mu$m and a pitch of 100 $\mu$m. An anode is placed below the GEM, with another voltage applied between the bottom side of the GEM and the anode, so the electrons are drifting to the readout structure, where they are detected. To achieve the desired gas amplification, one has to choose an appropriate detector gas. Such a detector gas consists mainly of noble gases since in contrast to molecular gases, the monatomic noble gases can not induce aging because nothing can decompose inside the detector. To suppress discharges in the gas, usually a so-called "quencher gas" like $CO_2$ is added to absorb photons that are produced by neutralizing the ions on the cathode.
To achieve higher amplifications, several GEM foils (usually 3) can be put on top of each other. The entire layout can be seen in figure 2.3, where one can also see the different steps of amplification in the 3 GEMs, while the field configuration is shown in fig. 2.4.
In this layout the incident electrons enter the detector on top through the cathode and are guided through the drift field to the first GEM, where the first amplification takes place. From there they are guided further down to the other GEMs and finally to the readout-plate on the bottom, where the charge will be collected and further amplified. This usually happens through several steps of pre- and other amplifiers, which will be described in detail later on. Depending on the layout of the anode, each signal can

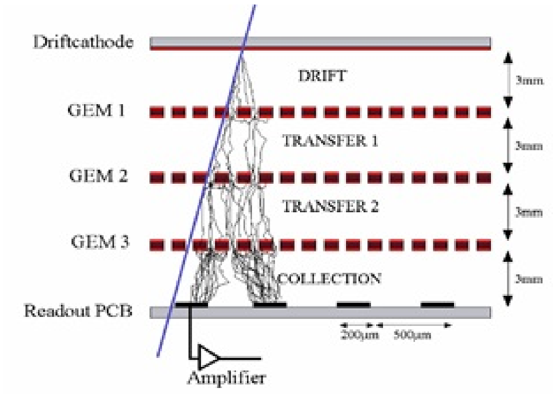


**Figure 2.3.:** Layout of a triple GEM [9]

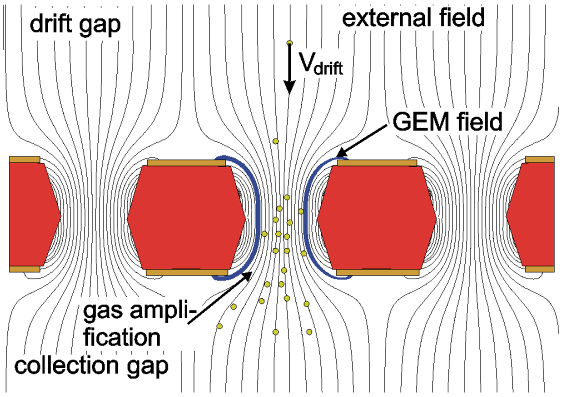


**Figure 2.4.:** Field configuration [10]

be assigned to a certain point in space and so a position-sensitive measurement is possible.
Since the pulse-height depends on the amount of charge deposited in the anode, a pulse-height analysis is performed where the peak amplitude is measured and then transformed to a digital signal in an analogue-to-digital converter (ADC). To cut off the low energy background (noise) a threshold is set to a certain level, below which no signals can pass. Finally the signal will be stored on a computer for further processing.

## 2.3. Pure Gas and Active Target

The main goal of this thesis is to show a possible operation of the triple GEM-detector with a pure gas instead of mixed gases like $ArCO_2$. To do that, the detector properties have to be well known to ensure a safe operation to avoid discharges with the risk of damaging the detector.
The reason for running the GEM-detector with pure gases is to use it in a future step as part of an active target GEM-based TPC ("Time Projection Chamber"). A TPC is a type of gaseous tracking detector with cylindrical geometry, which is usually aligned with the particle beam of the experiment (see fig. 2.5). The TPC is surrounding the interaction point where the beam hits the target. In this collision a lot of charged particles are produced, which enter the TPC and will ionize the gas atoms/molecules inside the chamber along their way. These ionized particles are then drifting to the readout pads, allowing for a 3-dimensional trace reconstruction (3rd coordinate = drift time) of the particles.
The idea behind an active target is to use the gas contained inside the TPC both as the tracking medium and as a low-mass reaction target, so charged nuclear reaction products can also be tracked and identified inside the target. For this to work, it is necessary to have very pure gases as well as a low-mass detector framework. The GEM

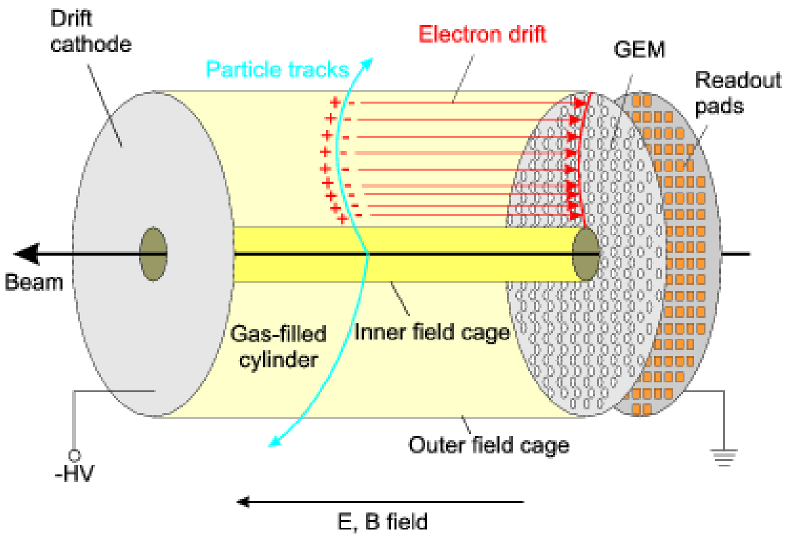


**Figure 2.5.:** Working principle of a time projection chamber [11]

detector, which is used for gas amplification, is filled with the same gas as the TPC and located on the base of the cylinder. The electrons will drift to the first GEM, where they are further amplified. In a triple GEM configuration this leads to an amplification factor in the order of 10,000.

# 3. Setup

## 3.1. Production of GEM foils

The first step in constructing a triple-GEM detector is the production of the GEM foils and subsequent mounting on a frame. The foils are usually manufactured at the CERN detector laboratory. The mounting is done by stretching a foil and then gluing a frame on it. The stretching is done in a device where the foil is stretched evenly on 8 points to ensure a consistent tension on all sides, as seen in fig. 3.1. High tension is necessary to make sure the foil will not deflect too much once an electric field is applied.
To investigate the effect an electric field will have on the foils we mounted tension load cells on 4 sides of our stretching device and measured the deflection of a 25 $\mu$m-thick foil for various forces. The assembly for that can be seen in fig. 3.1.

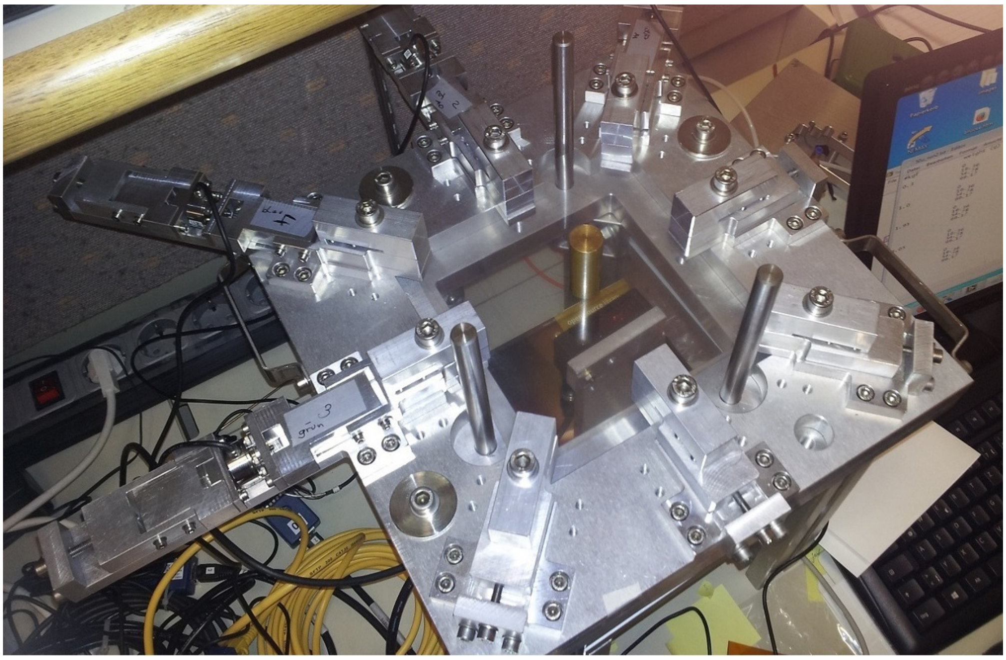

**Figure 3.1.:** Assembly for foil stretching and for deflection measurement

Once the load cells were calibrated, several tensions, corresponding to forces from 2.45 N to 36.30 N, have been used. For each of these tensions a deflection measurement was performed with an applied force on the foil between 0 N and 0.54 N. The result of these measurements can be seen in fig 3.2.

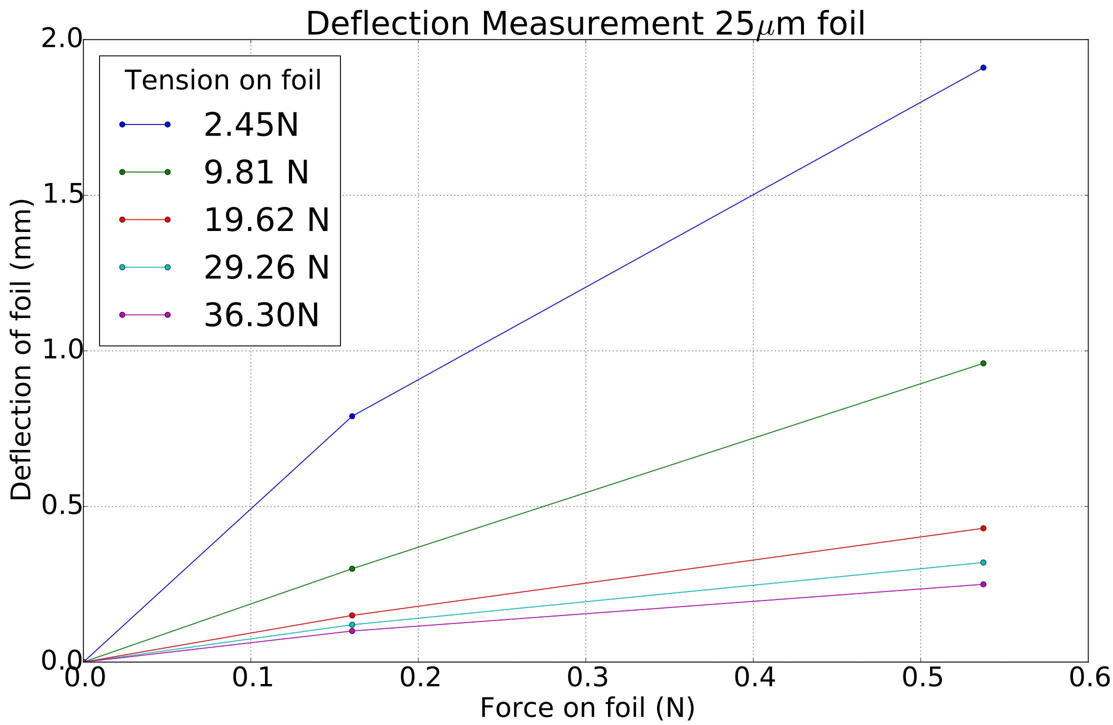


**Figure 3.2.:** Deflection measurements for 25$\mu$m foil

To set these values in a useful relation, it is necessary to know the present force inside the GEM-foils which can be calculated by assuming a parallel-plate capacitor:

$$F = \frac{\epsilon_0}{2} \cdot A \left(\frac{U}{d}\right)^2 = 9.58 \cdot 10^{-5} N \tag{3.1}$$

where U=400 V, A=25 cm$^2$ and d=4.3 mm. The value of the force applied through electric fields is way below the values we measured, so we can assume a deflection of D$\ll$ $100\mu$m for our future measurements. After showing, that the deflection of the foils is not going to be a problem, the foils can be glued to the frame and then mounted in the detector.

## 3.2. Triple GEM Detector

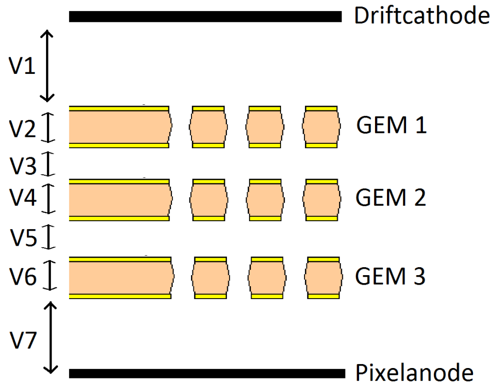


**Figure 3.3.:** Voltage regions inside the detector

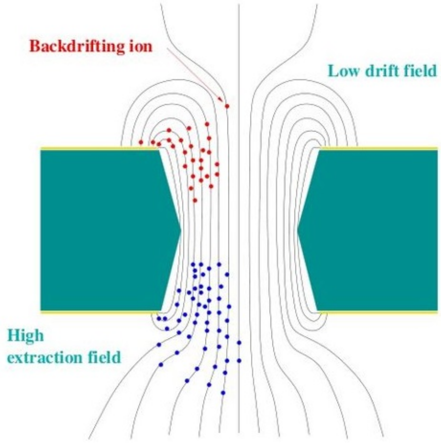


**Figure 3.4.:** Electron backflow after third GEM

For our measurements we used an already prefabricated device where up to 3 GEMs can be inserted on top of each other. With 3 GEMs there are seven different voltage regions $V_1 \ldots V_7$ (see fig. 3.3): $V_1$ above the first GEM, $V_2$, $V_4$ and $V_6$ between top and bottom of each GEM, $V_3$ and $V_5$ in between 2 GEMs and one final extraction voltage $V_7$ below the third GEM, which is usually higher than the other voltages to reduce electron backflow. This backflow is reduced at higher voltages since the electrons are accelerated stronger towards the anode. As mentioned before, the voltage in between a single GEM-foil should lie between 300 V and 400 V, so overall we applied a voltage of 2750 V to the upper drift cathode and a voltage of 670 V below the third GEM. This corresponds to a voltage of 347 V in each of the six regions $V_1 \ldots V_6$, which is achieved by a voltage divider (shown in appendix A), while the drift region $V_7$ has a higher voltage of 670 V.
The whole device, open and closed, can be seen in fig. 3.5. In the left picture, one can see the closed detector with a round kapton foil as window. For measurements, a radioactive source is placed on top of the foil, so the radiation can enter the detector directly above the cathode and the GEM foils. On the lower end of the device, there are 3 connections (see numbering in fig. 3.5). Port 1 and 2 are used to insert or remove the gas, respectively. Connection 3 is used to connect a vacuum pump. On the left side of the device, there are 3 voltage connections. The top one, number 4, is used as high voltage connector attached to the bottom side of the drift cathode, while connection 5 is wired to the lower side of the third GEM. Port number 7 is not used in this setup. Additionally, there are up to 40 outputs for readout-channels on each of the 4 sides, connected via IDE cables (number 6).

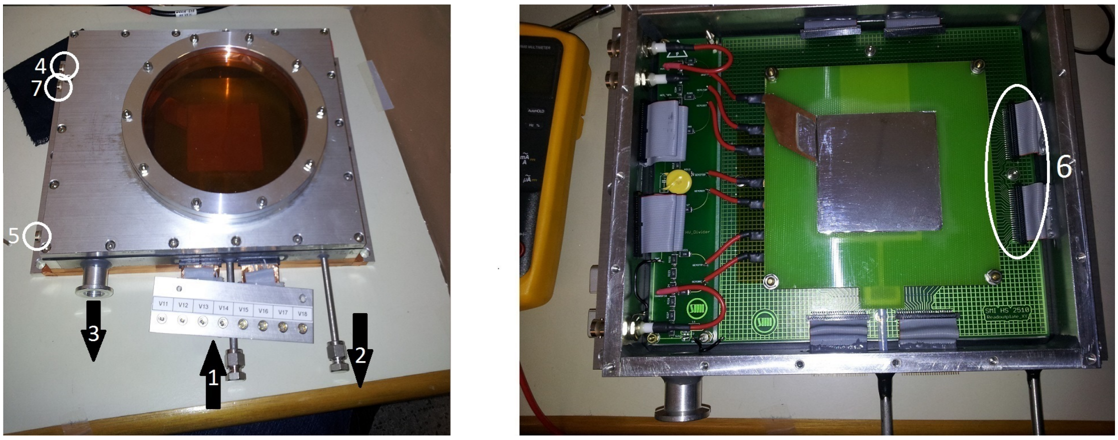


**Figure 3.5.:** Detector closed (left) and open (right). The tags 1 through 7 are explained in the text.

Inside the detector, the voltage divider on the left side of the device can be seen, connected to the top and bottom of each of the 3 GEM foils (red cables). These foils are not visible in the picture, since they are located below the silver drift cathode made out of aluminized Mylar. To ensure an even distribution of the gas throughout the detector, a grid was cut in the GEM frames where the gas enters the device and these foils. This grid is cut on the lower side of the green frame and can be seen in the right picture as a lighter green conduit below and above the cathode.

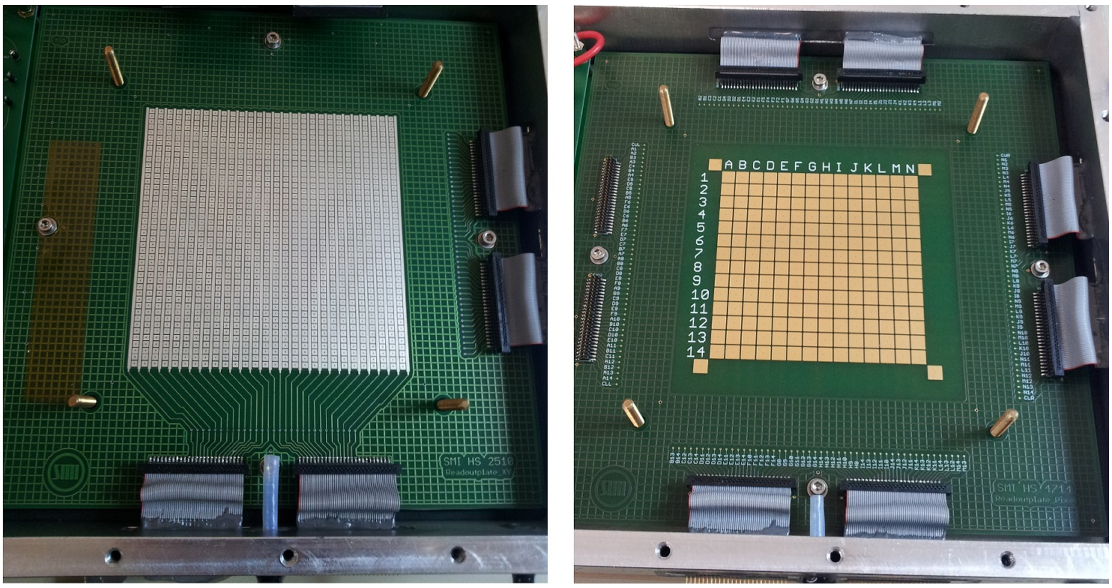


**Figure 3.6.:** Possible readout-structures: Strip anode (left) and pixel anode (right)

We decided to use an anode with pixel-readout and $16 \times 16 = 256$ channels (right side of fig. 3.6) and in this anode, each pixel is directly connected to one external channel. For our experiment we used 16 channels as shown in fig. 3.7, since all of those channels are connected to the same side of the detector, and therefore accessible through a single external preamplifier. The unusual numbering of the 16 channels is

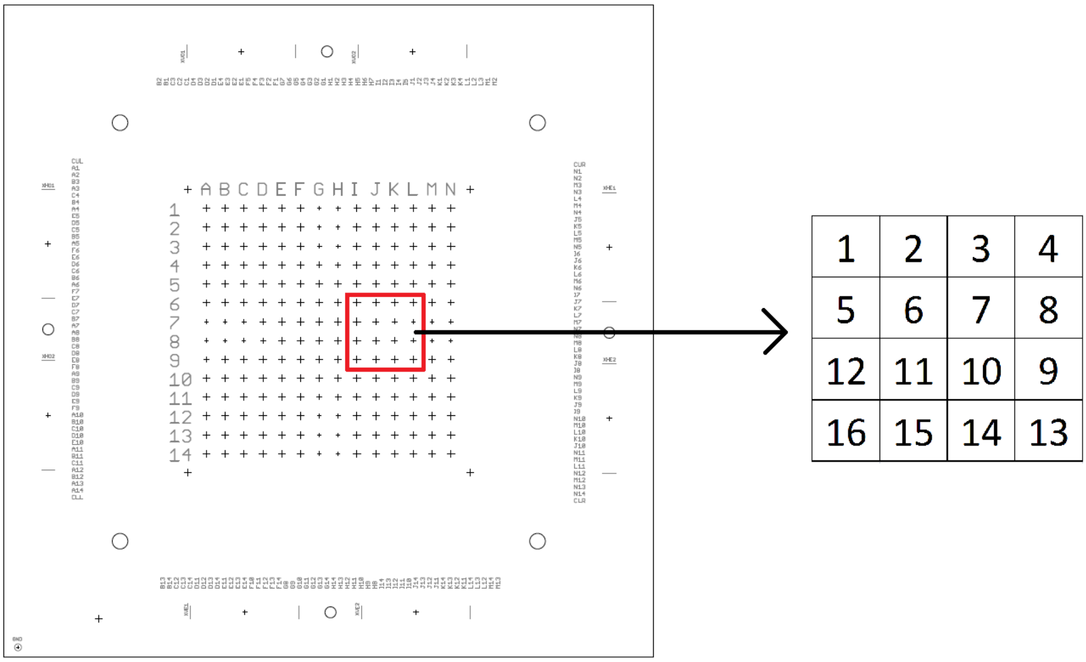


**Figure 3.7.:** 16 readout channels used in measurements

due to the internal wiring of the channels to their external connectors. With these 16 channels it is possible to check both the variations in amplification of several channels, crosstalk and/or signal splitting over several channels along a single line.

## 3.3. Preamplifier

We used a self-made amplifier with an amplification of about 250. To confirm this amplification-factor, a measurement was performed in which a capacitor with 0.68 pF capacity was charged with different voltages. Using this method a certain charge can be simulated, which is deposited on the preamplifier and can then be calculated via the relation $Q = C \cdot U$. The charge preamplifier is then used to amplify this charge and get a voltage-output. These values can be seen in fig. 3.8 and table 3.1.
This, together with the results from chapter 4.2 later on, where a deposited charge of 0.3 pC is calculated for a pulse-height of 1 mV, leads to an amplification of roughly

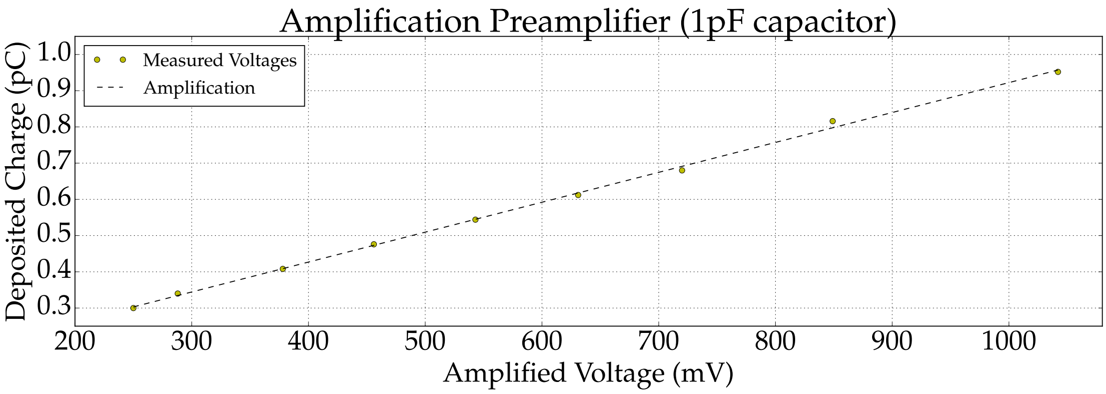


**Figure 3.8.:** Output Voltage compared to deposited charge in the preamplifier

| Dep. Charge (pC) | Meas. Voltage (mV) |
|---|---|
| 0.34 | 288 |
| 0.41 | 378 |
| 0.48 | 456 |
| 0.54 | 543 |
| 0.61 | 631 |
| 0.68 | 720 |
| 0.82 | 849 |
| 0.95 | 1042 |

**Table 3.1.:** Amplification of preamplifier for different deposited charges

250. As one can see in fig. 3.8, the charge/voltage ratio is almost linear over the necessary dynamic range.

# 4. Measurements

## 4.1. Measurements with $ArCO_2$ gas mixture

### 4.1.1. Preparations

One of the most commonly used gases in GEM detectors is a mixture of argon and $CO_2$ in various ratios. We used a so called "Ferromix C18" mixture, which consists of 82% Ar and 18% $CO_2$. Other common ratios are 90% Ar, 10% $CO_2$ or 70% Ar, 30% $CO_2$. The reasons for using this gas are its cheap price, relative fast drift time and the fact that due to the quenching gas $CO_2$ the risk of discharges is low. For the first measurements we used a voltage of 2600 V at the cathode and 600 V at the bottom of the third GEM. This corresponds to a voltage of (2600 V-600 V)/6 = 333 V in each of the regions $V_1$ to $V_6$ (see fig. 3.3) and a voltage of 600 V in region $V_7$. From now on, the voltages are always declared in a way that the first voltage outlines the voltage in between each GEM and therefore the value of the first 6 regions and the second voltage corresponds to the extraction region 7 (here: 333V/600V).

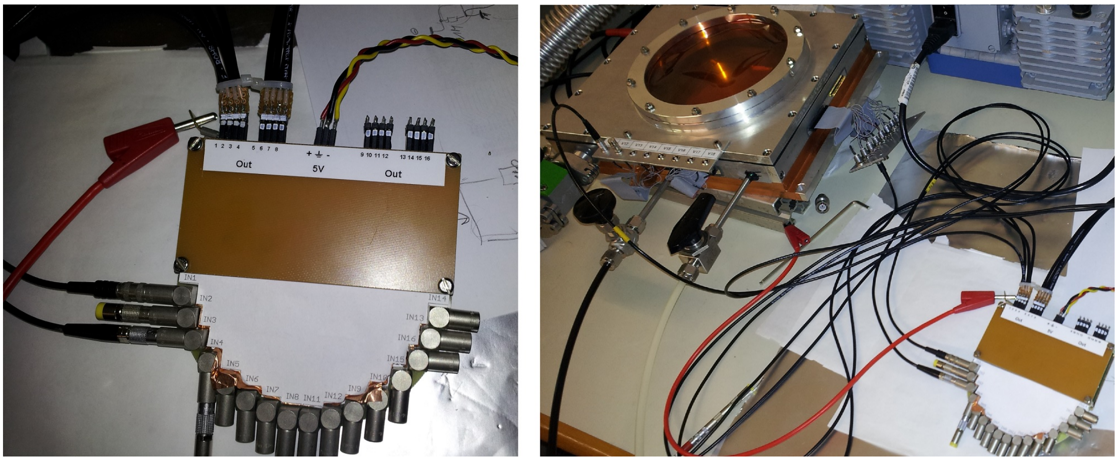


**Figure 4.1.:** First preamplifier (left) and connection to detector (right)

At first we used a setup with a 16 channel preamplifier (see fig. 4.1) which was not working properly, because this amplifier was connected to the detector through an extra set of cables, leading to extra background. To solve that problem, we immediately changed to a new setup, where we adopted a 16 channel preamplifier that can be mounted directly onto the detector to reduce background by using shorter cables. Another improvement was made to the shielding by screwing an aluminum plate on top of the preamplifier which was necessary because of the very thin, badly insulated cables connecting the detector and the preamplifier. The new setup can be seen in fig. 4.2. On the left side there is the new preamplifier with the cables connected directly to the detector, while on the right side the aluminum-plate is already attached. First measurements with this new preamplifier showed a sinus-shaped noise-pattern even without putting a radioactive source on top of the detector. The solution to this problem was a change of the decoupling capacitors in the preamp to filter out the low-frequency noise of the power supply.

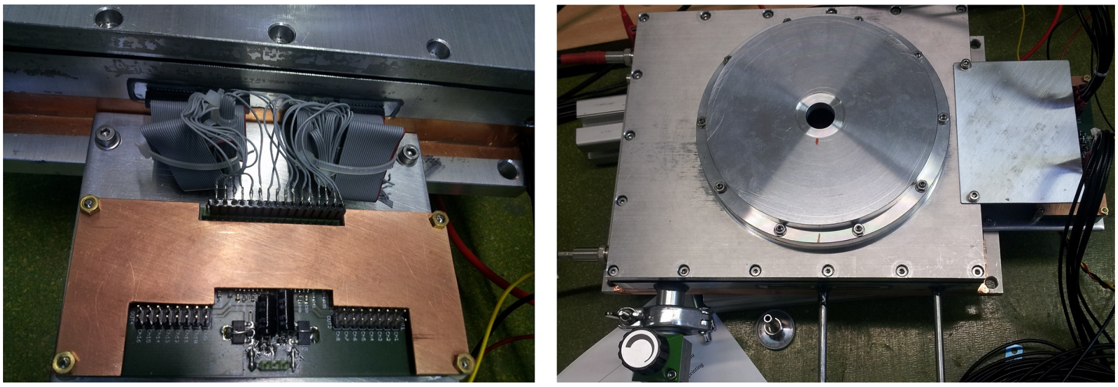

**Figure 4.2.:** Final preamplifier (left) and whole setup (right)

With these changes we could perform a first successful measurement. There was no longer any crosstalk between channels and we could see first events with a $^{137}$Cs-source. Our first measured signals, recorded directly from the oscilloscope, can be seen in fig. 4.3. In this picture, the measured channels are channel 13 (yellow, triggered in the left picture) and 14 (blue, triggered in the right picture), channel pattern as seen in fig. 3.7. In fig. 4.3, the left picture shows a small "bump" in the blue line, which means that some of the charge of channel 13 is deposited in channel 14. In the right figure, however, there is no signal splitting and all charge was deposited in channel 14. Once all these preparations were finished, we started a test to optimize the voltage settings. For that, the preamp was connected to a "Canberra 2020" spectroscopy amplifier to shape the signal in a Gaussian form which allows a better pulse height determination. This in turn was connected to a multichannel-analyzer (MCA, "AMPTEK MCA8000A"), which contains an integrated ADC and is connected via USB to the computer. In the MCA, the pulse height for each event is measured and then assigned to the appropriate channel, so in the end we have a histogram containing the number of pulses with the corresponding amplitude, a so-called "pulse height spectrum".

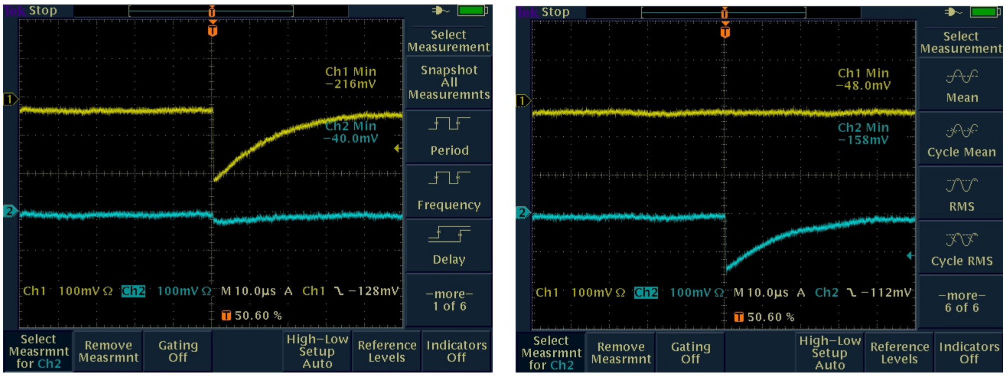


**Figure 4.3.:** First events measured with a $^{137}$Cs-source and ArCO$_2$ detector gas at 347V/670V. Left: Small crosstalk between channels. Right: No signal splitting

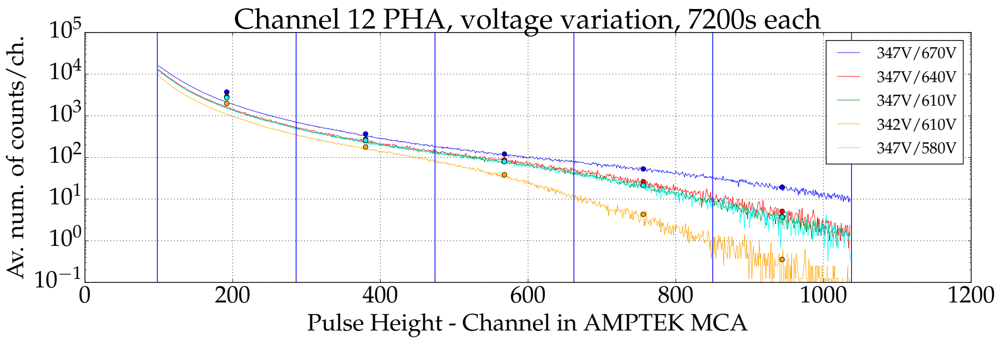


**Figure 4.4.:** Voltage variations with a $^{137}$Cs-source and ArCO$_2$ gas, each measured over 2 hours. Dots represent average over 190 channels. Due to the steep rise at the end, the first average is slightly shifted.

The AMPTEK MCA8000A has its own software for data acquisition and display (DPPMCA) and can therefore be used to create histograms on its own for each channel measured. Each measurement was performed over 2 hours using channel 12. The starting voltage was 347V/580V and after each run at least one of the voltages was raised to find the optimal voltage. For the results see fig. 4.4 and table 4.1. If one compares the 342V/610V gain with the 347V/580V gain (orange and cyan line in 4.4), it is easy to see that the latter has a higher gain, although the former has a higher extraction voltage. In this region the voltage between each GEM has a higher effect on the gain than the extraction voltage. If only the extraction voltage is raised by 30 V, as it is the case for the 3 measurements 347V/580V, 347V/610V, 347V/640V in fig. 4.4, there is not a big difference in the gain, until an even higher voltage of 347V/670V is applied, where once again a jump to a higher gain takes place. With this voltage of 347V/670V we found a good working point with no discharges. The 670 V drift

| Voltages | Sec. 1 | Sec. 2 | Sec. 3 | Sec. 4 | Sec. 5 |
|---|---|---|---|---|---|
| 347V/670V | 3723.5±4.5 | 366.1±1.4 | 120.7±0.8 | 53.0±0.5 | 19.4±0.3 |
| 347V/640V | 2870.9±3.9 | 272.6±1.2 | 86.5±0.7 | 26.2±0.4 | 5.1±0.2 |
| 347V/610V | 2728.7±3.8 | 256.3±1.2 | 79.7±0.7 | 21.6±0.4 | 3.8±0.2 |
| 342V/610V | 1977.3±3.2 | 178.1±1.0 | 38.4±0.5 | 4.3±0.2 | 0.4±0.1 |
| 347V/580V | 2713.7±3.8 | 256.2±1.2 | 79.9±0.7 | 21.3±0.4 | 3.7±0.2 |

**Table 4.1.:** Number of events from fig. 4.4, averaged over 190 channels each. Each section represents one of the regions in fig. 4.4 separated by vertical lines

voltage allows for a very good charge-collection. From now on for all measurements with $ArCO_2$, the applied voltage is 347V/670V, as represented by the blue line in fig. 4.4.

### 4.1.2. Single Channel Measurements

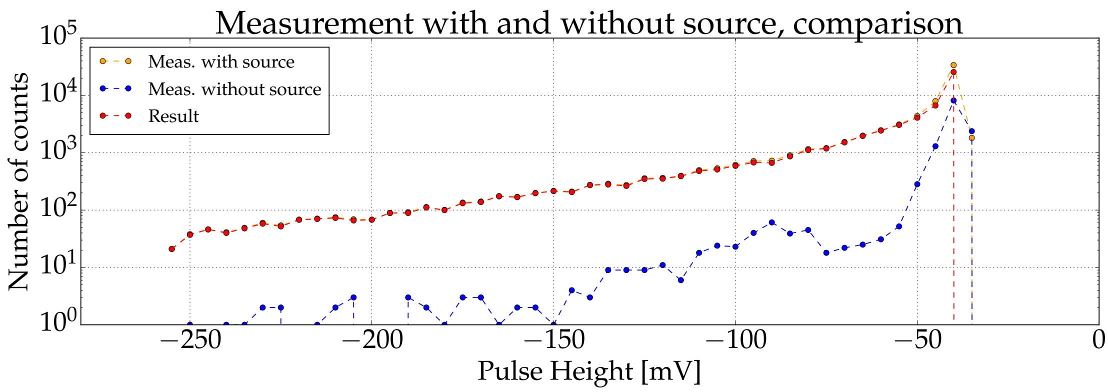


**Figure 4.5.:** Comparison of a measurement with and without source, "result" is the value with background subtracted. It clearly shows that the background has no influence, measurement without Canberra 2020 amplifier.

After establishing the suitable voltage at the end of sec. 4.1.1, we started measurements on all 16 channels. At first, however, we needed to determine the background level for our actual measurements. For that, we compared the events of a measurement with source to one without source. The result can be seen in fig. 4.5. It is clearly visible, that the background level for values below -50 mV is one to two orders of magnitude below that for actual events. This measurement showed, that the background did not influence our further measurement, so we will not take that into account. Each channel was measured separately over several 2-hour-shifts (at least 3), then a

histogram was produced to compare all channels with each other. The MCA8000A is set on 0-10 V Input range and 1024 channels, which means that channel 1024 corresponds to an input voltage of 10 V. The spectroscopy amplifier Canberra 2020 is set to an amplification of 30, so an event in channel 1024 of the MCA8000A corresponds to a voltage of 333 mV after the preamplifier.
For comparison of the individual channels we always clustered 4 of them, either along the vertical direction of the pixel anode, or along the horizontal direction. In fig. 4.6 one can see the channels 1, 2, 3 and 4 as indicated in fig. 3.7. In this graph, it is clearly visible, that channel 4 has a much lower gain than the other 3 channels. The same behavior is visible, if one compares the other channels along the horizontal direction.

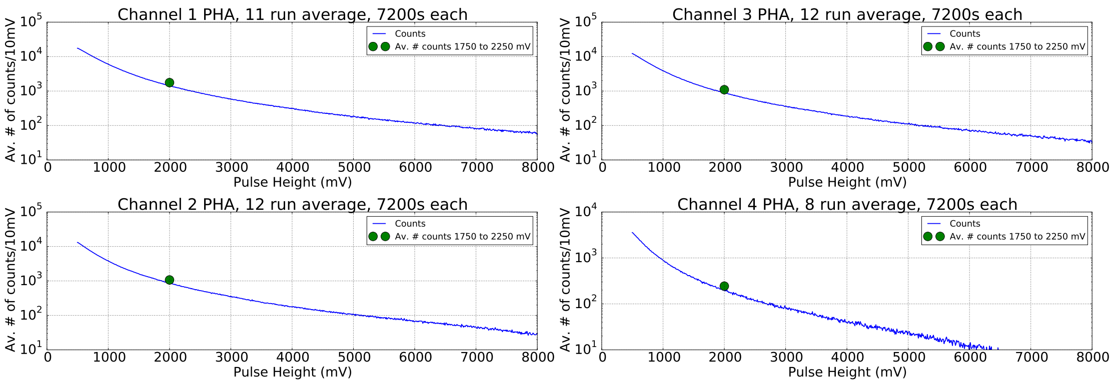


**Figure 4.6.:** Comparison of the gain of ch. 1 to 4. Note lower gain in ch4. Average counts from 1750 mV to 2250 mV: ch1=1756, ch2=1070, ch3=1095, ch4=244

The reason for this is our detector layout, in which the two outermost channels are partly covered by the G10 holding the GEM-foils. This may lead to a distortion in the electric field, which could reach a few mm inside the pixel anode and therefore affect the gain of the outermost used pixel in our setup. For clarification see fig. 4.7, where 2 pixels of the red pixel-anode are at least partly covered by the G10 (shaded area). This is why we decided to neglect the 4 rightmost channels in future measurements.
Now, if one compares the 4 channels 1, 5, 12 and 16, which lie in vertical direction to each other, the gain of all 4 channels is similar (up to 30%. . . 40%), as expected (see fig. 4.8). The graphs for each of the 16 channels can be found in appendix B.1.
To further compare the channels with each other, we summed over a pulse height region of 1500 mV, determined the average and plotted this value in the center of the summed range (see fig. 4.9).
A zoomed in version of this figure is shown in fig. 4.10. Here only the average over pulses between 1450 mV and 2950 mV is shown. The single channels are displaced horizontally for clarity, although all of them are summed over the same values.

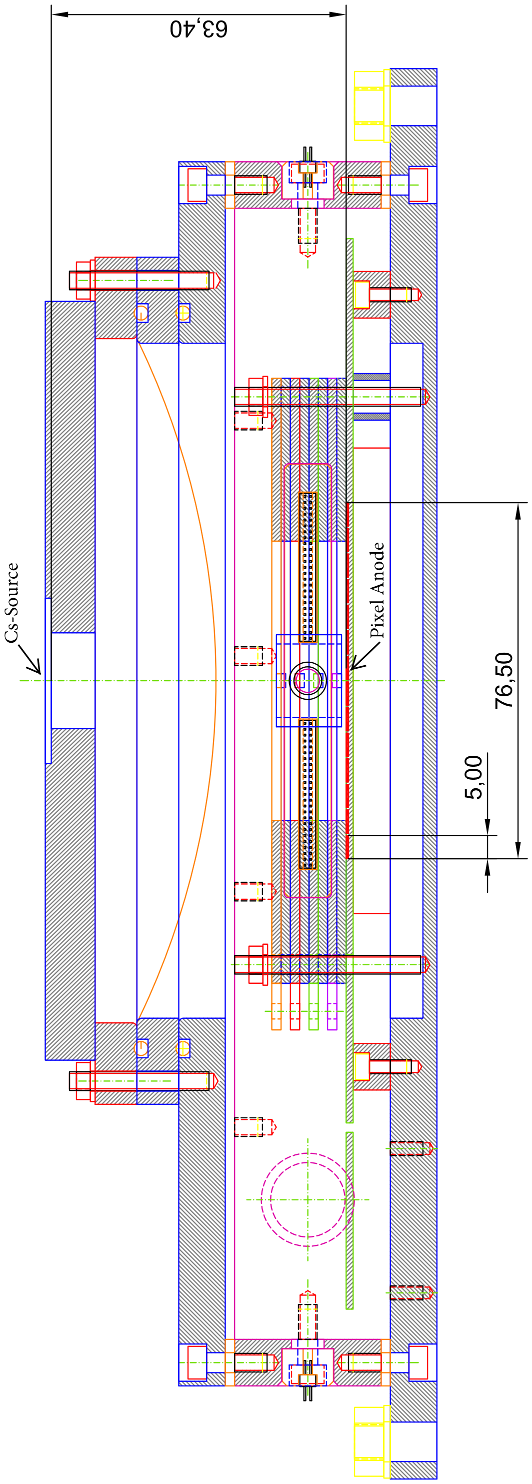


Figure 4.7.: Detector layout with pixel anode depicted. Note the 2 outermost pixel on each side lying below the plastic mounting shown as shaded area.

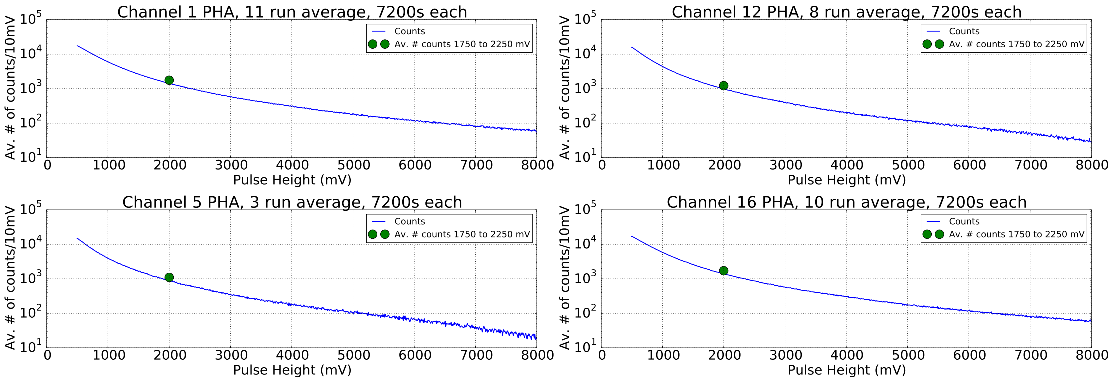


**Figure 4.8.:** Comparison of the gain of channels 1, 5, 12 and 16. Average counts from 1750 mV to 2250 mV: ch1=1756, ch5=1100, ch12=1223, ch16=1722. Ch1/ch16 still with impurity problems

With this analysis it is clearly visible that the 4 rightmost channels (4, 8, 9, 13) have a considerably lower gain than the other 12 channels. It is also notable, that channels 1 and 16 show a higher gain than the remaining 10. Those two were the first channels measured, and therefore the detector most likely still contained a considerable amount of impurities like oxygen and $H_2O$. Since the ArCO$_2$-detector gas is continuously flowing through the chamber, the purity of the gas inside the chamber gets higher with time.

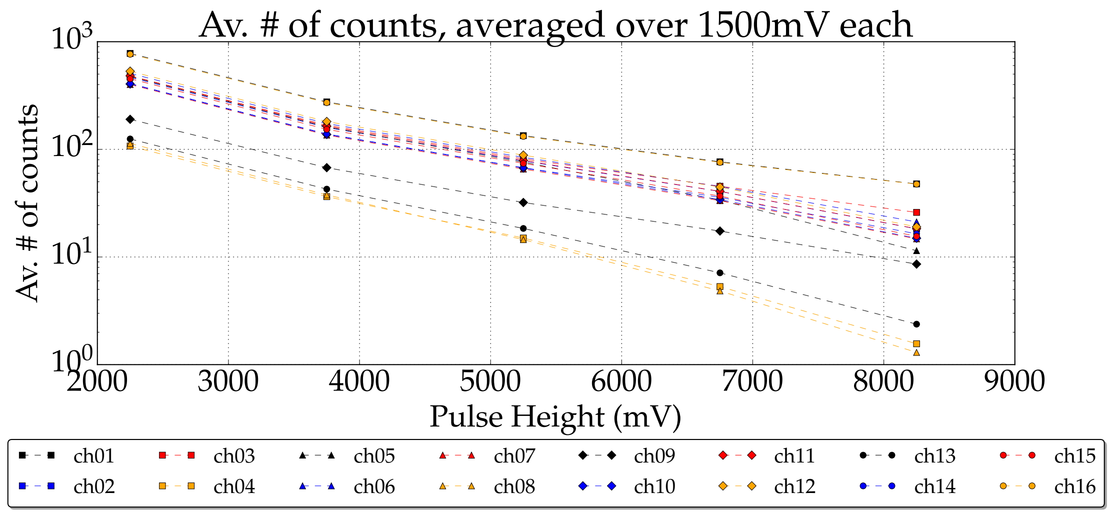


**Figure 4.9.:** All channels compared, each summed over 1500 mV. The channels 4, 8, 9 and 13 show much lower gain than the rest.

The measurement for all channels lasts over a period of one week. To check the

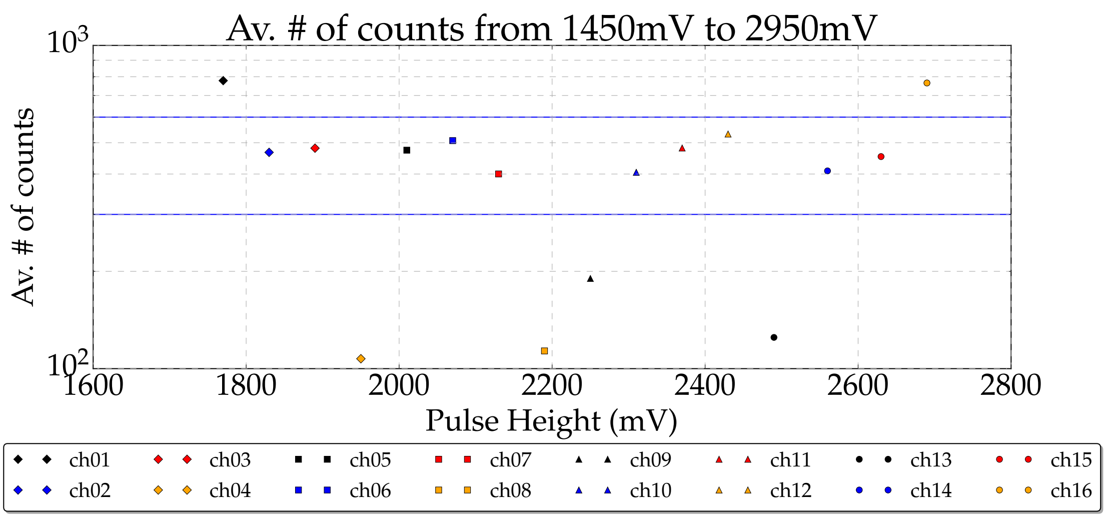


**Figure 4.10.:** Zoomed in version of fig. 4.9, voltage region 1450 mV to 2950 mV. Single channels are displaced horizontally for better clarity. Note lower gain of ch. 4, 8, 9 and 13 and the higher gain of ch. 1 and 16.

measurements for consistency over short periods of time, a further analysis of the data for one of the channels (channel 2) was performed. For this channel, there are 10 runs over 2 hours each, so it was possible to compare each run to the average over all 10 runs to see, if there were any big deviations over shorter time periods. The data is presented in fig. 4.11. For a more details of fig. 4.11 as well as zoomed in figures for the other regions, see appendix B.2. In these figures, the average number of counts is depicted with their $3\sigma$-error-bars, and it is clearly visible that almost all of the single 2-hour measurements lie within these error-margins consistent with statistical predictions, showing that the systematic uncertainties are small. To make sure that the measurements are stable over larger time scales, a second measurement of channels 1, 5, 12 and 16 was started one week after the end of the first one. For a comparison between the two runs see fig. 4.12. Before this second run was started, the detector chamber was evacuated to ensure optimal conditions, with an impurity level as low as possible. Each channel in this second run was measured for at least 4 hours (2 runs of 2 hours each). To compare these second runs to the first runs, once again they were summed by averaging over a range of 1500 mV, so there is an average number of counts for 1450. . . 2950 mV, one for 2950. . . 4450 mV and so on. For clarity, each channel in fig. 4.12 is displaced to each other horizontally, although all of them are summed over the same values. In this graph, it is clearly visible, that channels 1 and 16, which in the first run showed a higher gain than the other channels, are now at the same level, so the aforementioned assumption of impurities in the chamber is reaffirmed.

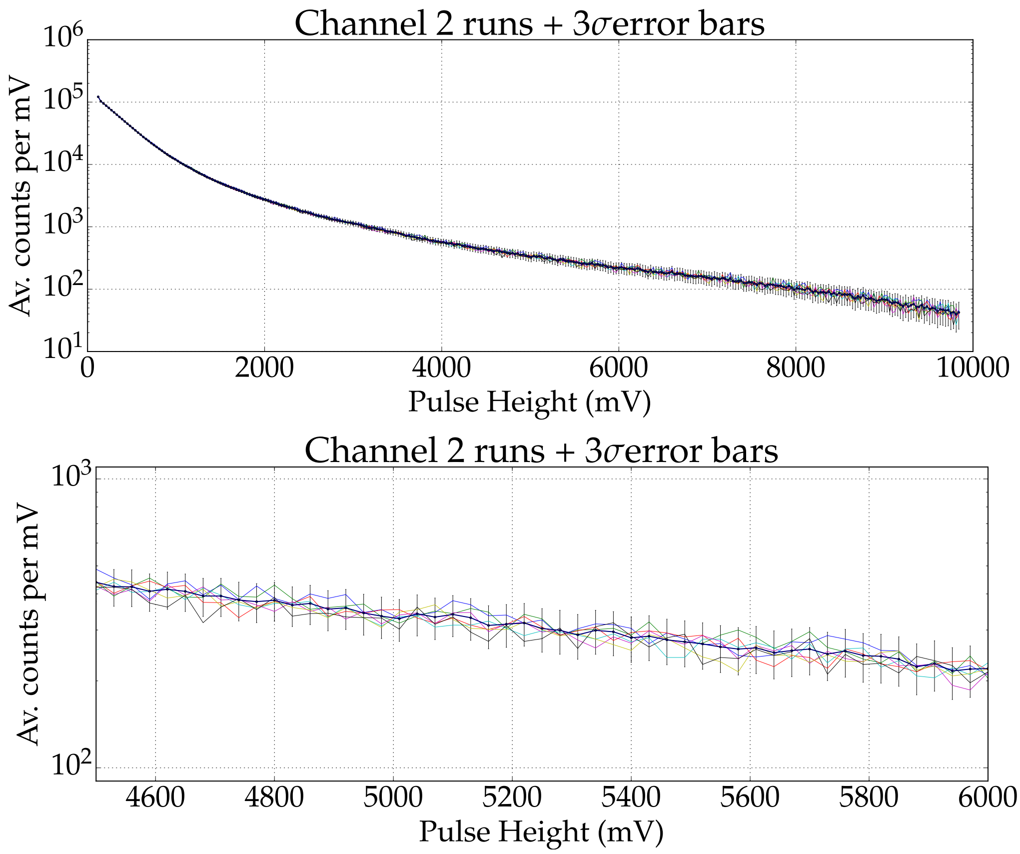


**Figure 4.11.:** Channel 2 average with $3\sigma$ error together with values for 10 single runs (top). The $3\sigma$ error-region of our plot contains over 99.7% of the events, consistent with statistical predictions. Zoomed version (bottom), 1500 mV range for better visibility.

All channels have now been measured and compared to each other, so it is now safe to say that, except for the 4 rightmost channels, all other channels have comparable gain if a certain low impurity level is achieved. It is possible now to do multichannel measurements, where one channel with the highest pulse height is selected and displayed with the other ones. Therefore it is possible to take a look at the crosstalk between channels and to determine the charge-distribution between two channels.

## 4.1.3. Multichannel Measurements

To measure several channels simultaneously, it is necessary to replace the previously used AMPTEK MCA8000A containing only a single ADC with a new multichannel

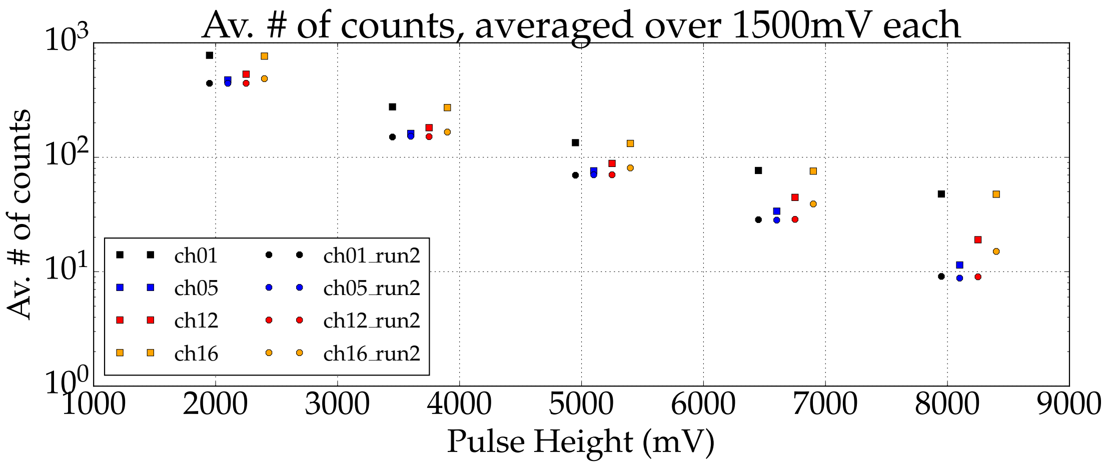


**Figure 4.12.:** Comparison of the gain of 4 channels for 2 different runs. Each channel is summed over the same 1500 mV values from 1450 mV to 2950 mV, 2950 mV to 4450 mV and so on. In run 2, the pulse height for all 4 channels is at the same level

ADC. We used a quad 8k ADC ("Ortec AD413A") together with a CC-USB Controller ("Wiener CC-USB"), both housed in a CAMAC crate which is connected to a computer. To be able to use the quad ADC, a certain setup as seen in fig. 4.13 is necessary. The following parts are used in this setup:

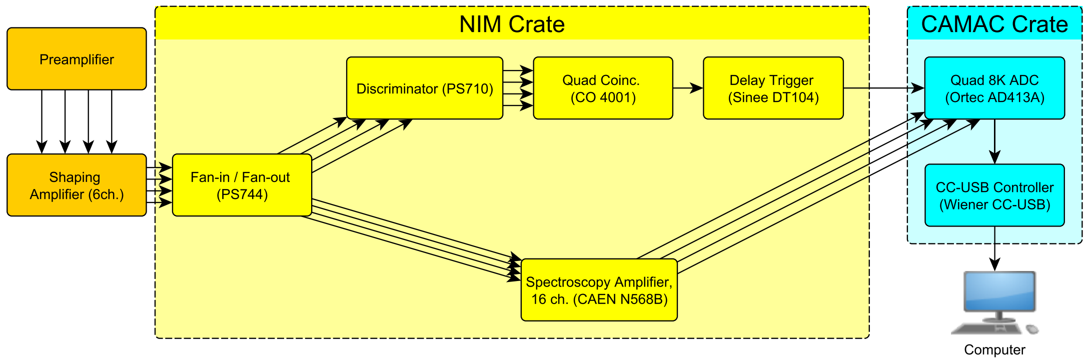


**Figure 4.13.:** Measurement chain for quad channel measurement, "upper path" for trigger, "lower path" for signal, each arrow represents one data link

- Preamplifier: This is the same 16-channel preamplifier as in the single channel measurement

- Shaping amplifier: Instead of the Canberra 2020, which is just a single channel amplifier, we now used a self-built shaping amplifier as an intermediate step.
- Quad linear Fan-in/Fan-out gate, "Phillips Scientific PS744": Needed to split the signal of each channel without loss of signal-height. This Fan-in/Fan-out delivers one inverted output, which is connected to the spectroscopy amplifier and one unchanged output used to create a trigger for the ADC.
- Octal discriminator, "Phillips Scientific PS710": This discriminator allows to set a threshold and adjust the width and delay of the logic output signal of the discriminator for each channel separately.
- Quad coincidence unit, "CO 4001": The logic device allows to combine channels via an or-gate. At first, 2 times 2 channels are connected in one or-gate, and the result of both is connected in another or-gate.
- Delay trigger, "SIN DT104": To make sure that the trigger signal is long enough, an additional delay trigger was implemented after the or-gate, which is then used to control the ADC.
- Spectroscopy amplifier, "CAEN N568B": The signal path goes through this amplifier with adjustable shape, coarse and fine gain and offset.
- Quad 8k ADC, "Ortec AD413A": The 4 outputs from the CAEN spect. amplifier are connected to the 4 inputs of the "Ortec AD413A", where each input has a range from 0 to 10 V and the analog signal is converted to a digital signal.
  The trigger is forwarded to the integrated ECL (= emitter-coupled logic) gate and controls the conversion from the analog input to the digital output.
- CC-USB Controller: Since both the Ortec Quad 8k ADC and this Wiener CC-USB are implemented in the CAMAC crate, they are connected internally, so no extra connections are necessary. The CC-USB is then connected to the computer, where a software can read the incoming signals and write them in a text-file, separated by channels. Each time a trigger signal above threshold is detected all 4 channels are recorded.

To get a better idea of how the signals look like after each amplifier stage, fig. 4.14 shows all 3 stages. The top picture shows the signal directly after the preamplifier. In this stage the signal is only amplified but not shaped. The shaping process starts with the shaping amplifier in the middle picture, where one can see how the shaping works, making almost a Gaussian signal. Finally, the spectroscopy amplifier, as seen in the bottom picture, has to invert the signal since the ADC can only work with positive input. Note the different vertical scales in the 3 figures between 10 mV/div directly after the preamplifier and 500 mV/div after the spectroscopy amplifier. Note also the different time-bases between the first figure and the other two.

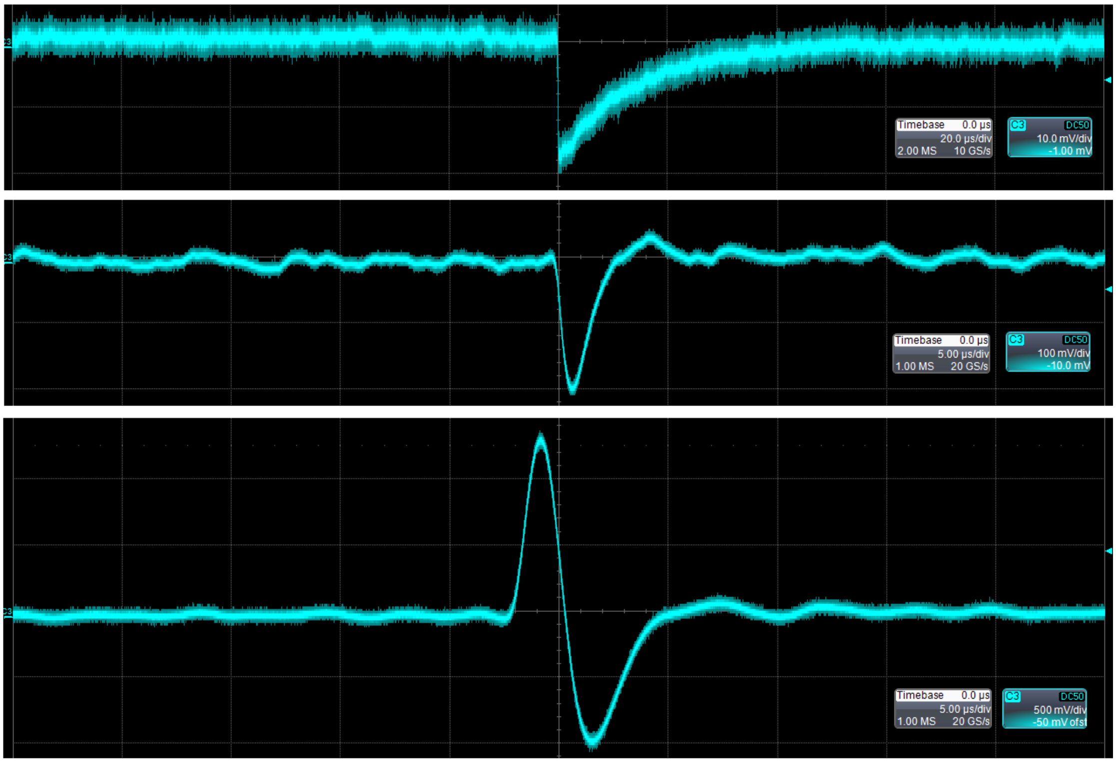


**Figure 4.14.:** Signal shape after different amplifier stages: Preamp. (top), shaping amp. (middle) and spectroscopy amp. Last signal has to be inverted for the ADC to work. Note different time-base and vertical range

To further process the data, each data-file is analyzed in a way that for each trigger event the channel with the highest voltage is seen as the main event while the other 3 are seen as secondary events. In this way it is ensured that the channel with the highest deposited charge is seen as main event, even if the incident particle was emitted in an angle so that an event is detected in more than one channel. Another possibility for events in more than one channel is the fact, that when the electron avalanche takes place in the GEM foils it is spread out over a certain space and it can happen that depending on the position, charge is deposited in more than one channel (compare fig. 2.3). The next experiment was done by performing measurements through different combinations of channels. We started with measurements along the vertical channels

| | | | |
|---|---|---|---|
| 1 | 2 | 3 | 4 |
| 5 | 6 | 7 | 8 |
| 12 | 11 | 10 | 9 |
| 16 | 15 | 14 | 13 |

**Figure 4.15.:** Ch. layout anode

1, 5, 12, 16 followed by channels 2, 6, 11, 15 and then channels 3, 7, 10, 14. The 4 rightmost channels were not measured because of the known problem of the field-deflection at these channels. Nevertheless, we still performed one measurement along the horizontal line of channels 5. . . 8 to confirm this fact once more. For convenience, the channel layout is again depicted in fig. 4.15. Each measurement was 24 hours long. Two of the triggered channels (6 and 8) from the measurement along the horizontal channels 5 to 8 are shown in fig. 4.16.

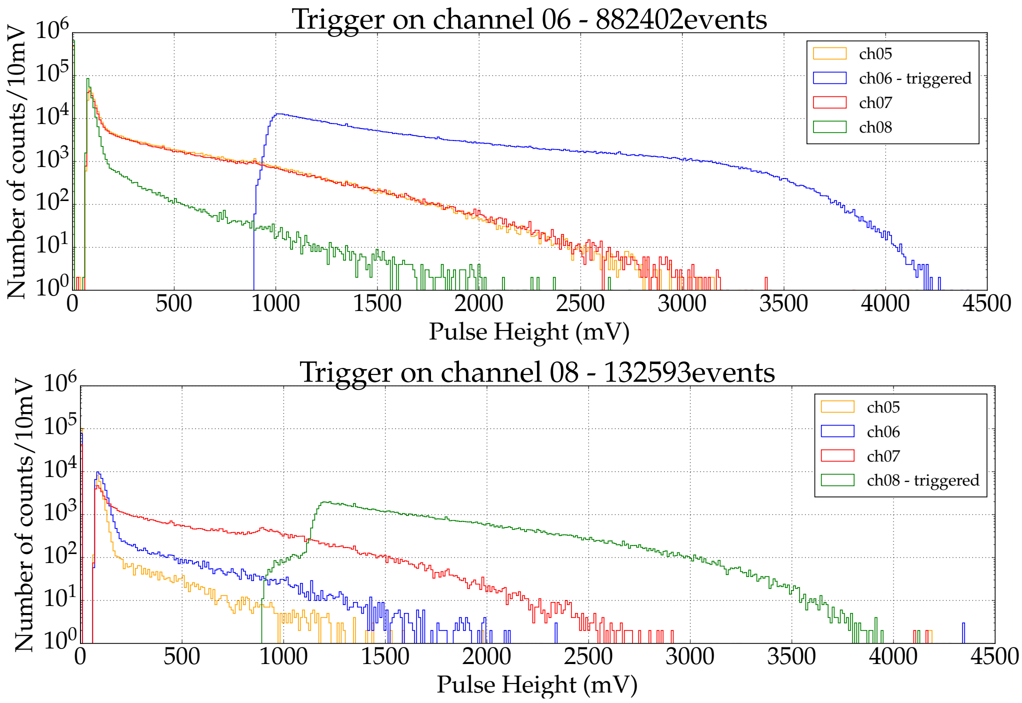


**Figure 4.16.:** Quad channel measurement along channels 5 to 8, triggered on channel 6 (top) and 8 (bottom). Note the amount of events in channels adjacent to triggered channel. In top picture, both ch. 5 and 7 have almost the same gain. Note also the bump of channel 8 in the lower figure, hinting a problem with the trigger.

The most important thing to notice here is the difference in the number of events. Channel 8 in the lower picture has less than a sixth of the counts of channel 6 in the upper picture, although both were triggered. This is expected, because channel 8 is one of the outermost channels, as explained before. The second thing to notice is the fact, that our trigger on channel 8 doesn't seem to work properly. This is a problem of the PS710 octal discriminator, which has at least 3 of its 8 channels not working correctly, so they are either unstable or can't be adjusted at all. This was only found out after this measurement, which we corrected for the next runs. The remaining two

measurements are not shown here.
Since the channels 2, 6, 11 and 15 (second column of channels) have been measured over 3 days during the weekend (Friday 4pm to Monday 10am), we split them up in 3 runs of equal length of 22 hours each to compare them with each other. Let's first take a look at one channel in one of these runs. For a better comparison of the total intensity of each channel, in fig. 4.17 the average over 500 channels each was calculated and plotted for the case where channel 2 is triggered.

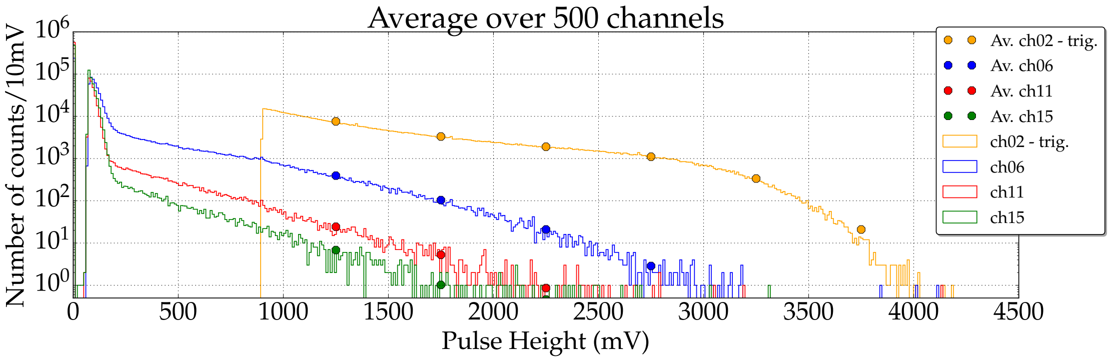


**Figure 4.17.:** Trigger on channel 2, together with average over 500 mV each. Note the low amount of events for not triggered channels, especially above 3000 mV. Average number of counts for pulse heights 1000 mV to 1500 mV: ch02=7594, ch06=393 ch11=24, ch15=7

In this graph it is clearly visible that events above 3000 mV are seen almost exclusively in the triggered channel. The maximum voltage in a single channel is at about 4000 mV. Nevertheless, some of the split signals have to have a higher total energy than that, since there are signals of up to 3000 mV in channel 6. This means that, at the same time, the event in channel 2 had to be above these 3000 mV, or the trigger would have switched to the other channel. Still, on average only 2 events are seen per mV in the range between 2500 mV and 3000 mV on channel 6, compared to a total of over 850.000 events. One possible explanation for those high energy events might be accidental coincidence of a cosmic particle with a trigger event.
In fig. 4.18 one can see all 4 channels of this run. The trigger was set to 900 mV, which also corresponds to channel 900 in the quad ADC, since the amplification was calibrated accordingly. The trigger had to be set for each channel manually, so small deviations in the trigger level between channels are possible. In the 4 graphs of fig. 4.18 it is clearly visible that in all 4 cases the triggered channel shows the highest number of events for each value above 900 mV, as expected. What can be seen as well is the fact, that each channel further away from the triggered channel has a lower intensity than the channel closer to the trigger. So, for example in the first graph, the blue channel 6, which is located directly below the triggered channel 2, shows a higher

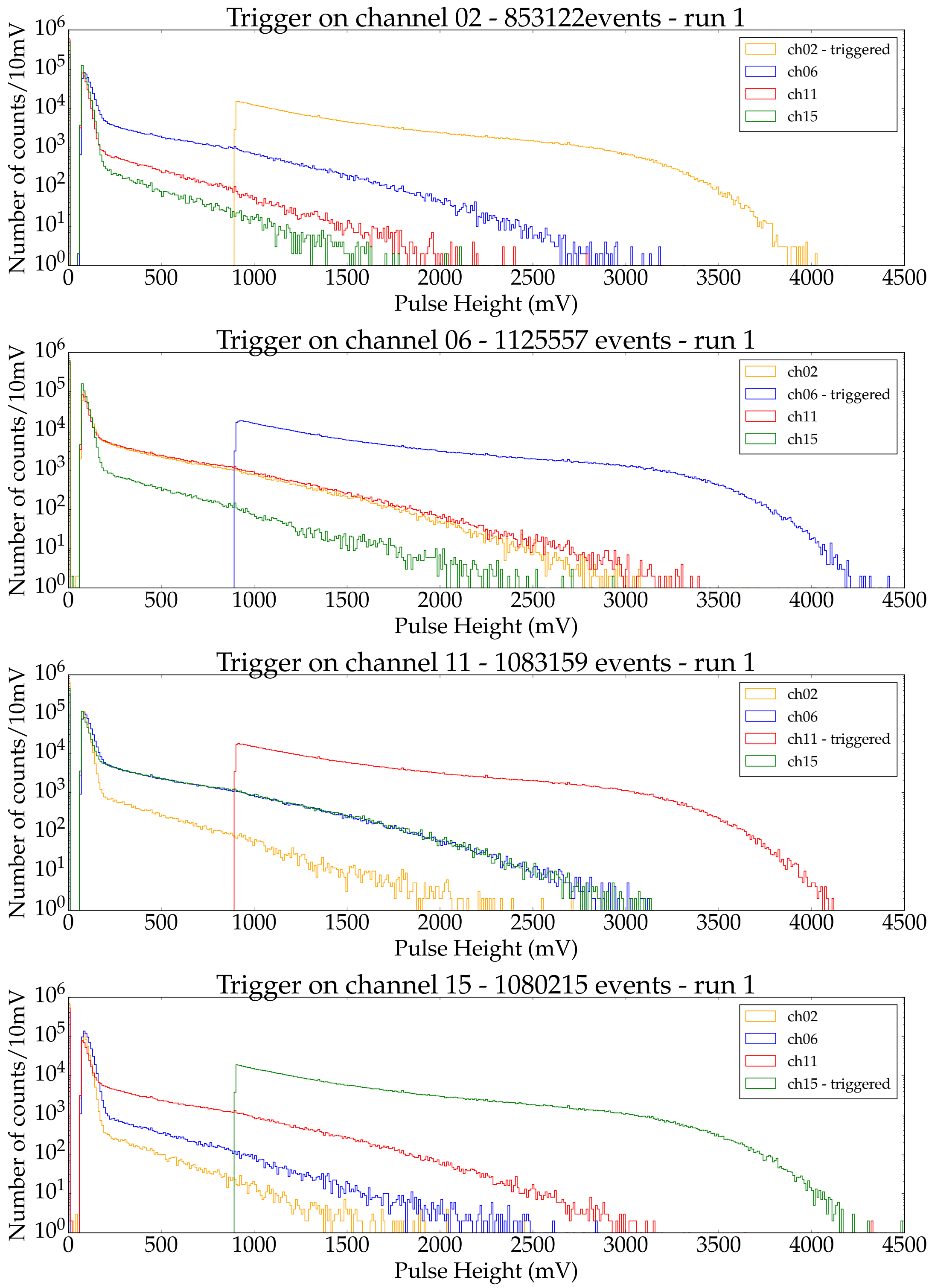


**Figure 4.18.:** Quad channel meas. along ch. 2, 6, 11, 15, each triggered channel in one figure. Note similar gain of channels in second, third and fourth figure and lower gain in first figure (pulse heights 4000 mV to 4500 mV), leading to lower intensity

intensity than channel 11 (red) and even more so than channel 15 (green), both of which are located further away from channel 2. Also, in the next two graphs, where the trigger is placed on channels 6 and 11, respectively, one can see that both times the two channels directly above and below the triggered channel show almost exactly the same intensity since the charge has to be split symmetrically. This is a good evidence for the fact that all these channels are working as expected. One last thing to notice is the different amplification in the 4 channels. While channel 2 has its maximum at around 3800 mV, channel 11 has the maximum at 4100 mV and the two channels 6 and 15 at around 4300 mV . This is the reason for the lower intensity of channel 2 compared to the other channels.
We then compared all 3 runs of these channels with each other to see, how stable the setup is. To do so, the normalized average over all 3 runs was calculated for each channel separately. The results can be seen in fig. 4.19. In this figure, once again the average over 500 mV was calculated, as in fig. 4.17, and then normalized. The average for all channels is always at the same pulse height, but in the graph they were shifted horizontally to each other for clarity. All channels were averaged over voltages from 1000...1500 mV, 1500...2000 mV and 2000...2500 mV. The most important thing to notice here is, that in each measurement the triggered channel shows the least deviation, as expected. It is also noticeable that the deviations from 1 grow with the pulse height, which is also expected, since the number of counts is lower for these regions. To get a better understanding in how reliable the measurements are, we displayed the error-bars for a normalized averaged data-set, as seen in fig 4.20. Here channel 11 is triggered and the indicated error-bars are the $1\sigma$ errors for each measurement. For clarity only one specific value is picked out, in this case the average over the values from 1000 mV to 1500 mV. The $3\sigma$-error values for each of the 4 channels can be seen in appendix B.3.
Even with just $1\sigma$ error bars, all values lie within each others error, at least up to 2500 mV. For higher voltages, this is no longer the case, but almost all of the measurements lie within the $3\sigma$-error-margin (see appendix B.3).

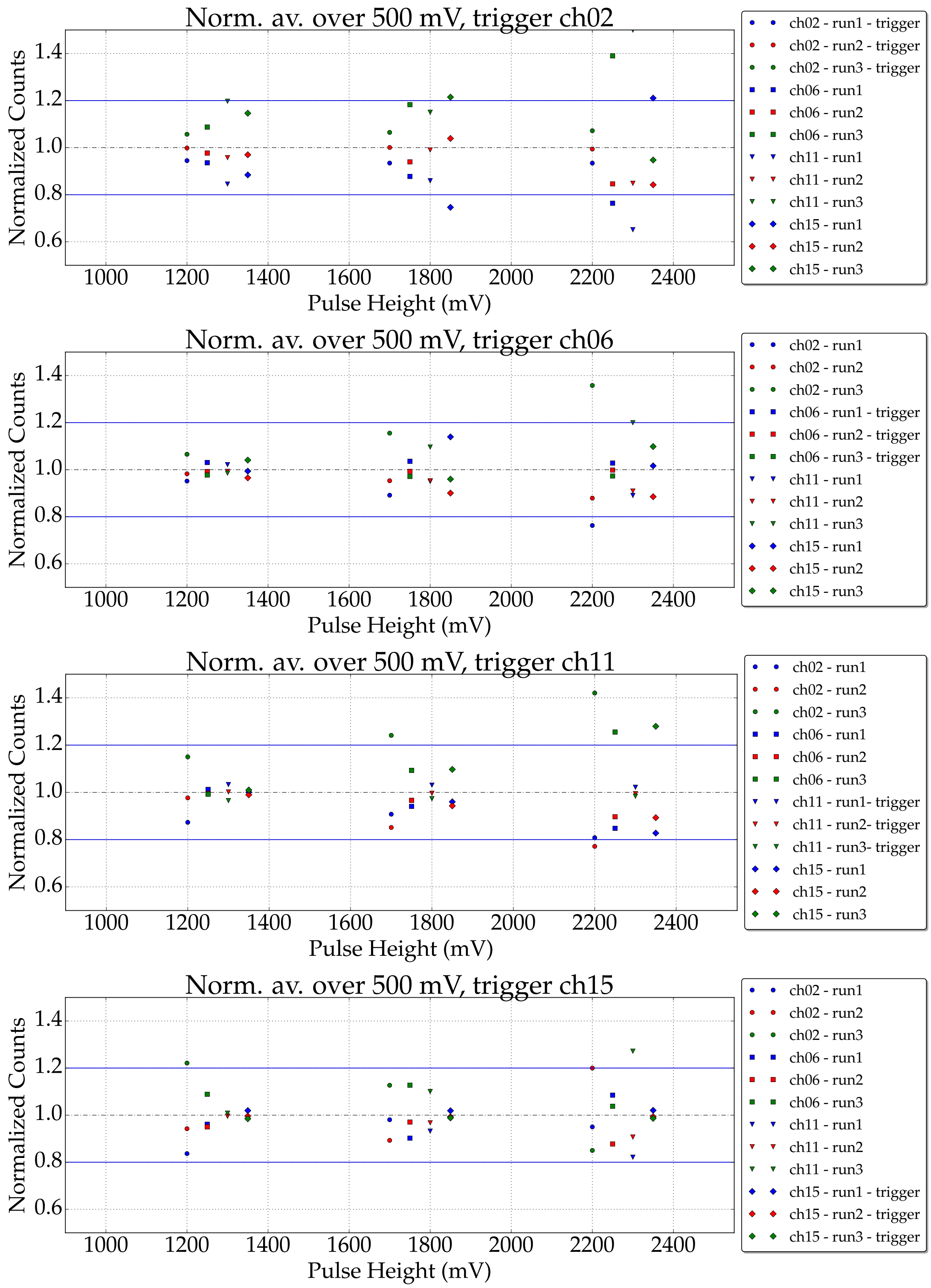


**Figure 4.19.:** Normalized average of all 4 channels over 3 runs. All summed over same voltage-region (1000 V to 1500 V, ...), shifted horizontally for clarity

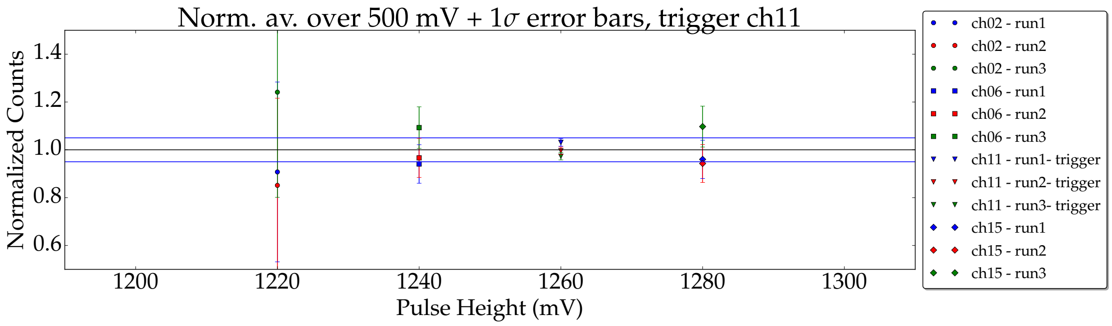


**Figure 4.20.:** Normalized average + $1\sigma$ error bars for 1000 mV to 1500 mV, triggered on ch. 11. All values within error margin. For the triggered ch. 11, all 3 runs within <±5%, as indicated by the horizontal lines

## 4.2. $^{55}$Fe-Measurement

To determine the gain of our triple GEM, we used a $^{55}$Fe-source, which emits K-alpha X-rays with an energy of 5.9 keV at a probability of 24.4% and K-beta X-rays with an energy of 6.5 keV at a probability of 2.8%. Since these energies are so similar, our resolution is not high enough to distinguish between the two lines.
We measured the spectrum of these X-rays for a voltage of 367V/500V over two hours and calculated the effective gain from the measured spectrum. To implement the $^{55}$Fe-source into the detector, in a first test we put in a fourth framed kapton-foil on top of the 3 GEMs, on which the $^{55}$Fe-source was laid. In that way the $^{55}$Fe lies directly on top of the detector in order to get a higher amount of photo-electrons. With this setup, however, there was a problem with changes in the rate of events over short time periods, which was not noticed in the beginning. After another measurement with pure argon as explained later, where this problem is addressed, a new $^{55}$Fe measurement has been performed. In this experiment we used a stronger source, so we could put it on top of the detector instead of inside, which does not lead to the mentioned problem. With this new setup we could get the spectrum seen in fig. 4.21. One can see a clear peak in this figure at around -18.5 mV, which means that a photo-electron was produced and stopped completely in the gas of the drift volume.
After recording the pulse height spectrum, another measurement was performed by directly measuring the voltage on an oscilloscope with a 1 MΩ internal resistor. In this measurement a voltage of 1 mV was measured, which leads to a current of

$$I = \frac{10^{-3}V}{10^{6}\Omega} = 10^{-9}A. \tag{4.1}$$

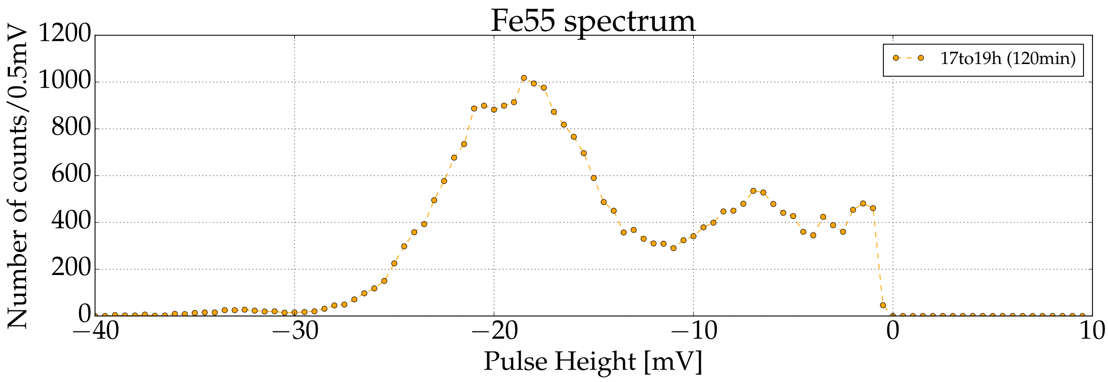


**Figure 4.21.:** Pulse height spectrum of $^{55}$Fe over 2 hours. Clearly visible peak at -18.5 mV means full ionization

With a pulse duration of 0.6 ms and assuming a triangular pulse-form, this corresponds to a deposited charge of

$$Q = 0.5 \cdot 0.6 \cdot 10^{-3} s \cdot 10^{-9} A = 3 \cdot 10^{-13} C. \tag{4.2}$$

One electron carries a charge of $1.6 \cdot 10^{-19} C$, so this corresponds to

$$N = \frac{3 \cdot 10^{-13} C}{1.6 \cdot 10^{-19} C} \approx 2 \cdot 10^6 \tag{4.3}$$

electrons. To get the effective gain of the 3 GEMs, this value has to be divided by the incident ionization in the gas. Since the X-rays of the $^{55}$Fe-source have such a low energy, the range of such a photo-electron is less then 1 mm. Therefore we can assume a full ionization, corresponding to 200 electrons between the cathode and the first GEM. With this, we can now calculate the gain of the triple-GEM detector. The gain over all 3 GEMs is

$$\frac{2 \cdot 10^6}{200} = 10,000 \tag{4.4}$$

giving a gain of about 20 electrons per GEM.

## 4.3. Pure Gases

### 4.3.1. Helium

Once the runs with $ArCO_2$ were finished, we started measuring pure gases. As mentioned before, in our setup we need pure gases to use the detector as an active target. As a first test we decided to use helium. In this first run, however, discharges occurred as soon as we reached a voltage of just 150 V in between the different GEM-regions. After disassembling the device to check for dust-particles and other pollution on the foils, we did a measurement on the GEM foils themselves to see, if any current is flowing through them. If so, they would have to be replaced, since the upper and lower copper-plate of each GEM should be separated with an insulating kapton-layer in between. It turned out that the GEM foils were fine, but in the previous measurement-process one of the cables connected to the voltage divider were loose, so we replaced these cables with more flexible ones. After reassembling the detector, another test was performed. There were still no improvements on the discharges, as soon as the voltage exceeded 150 V.

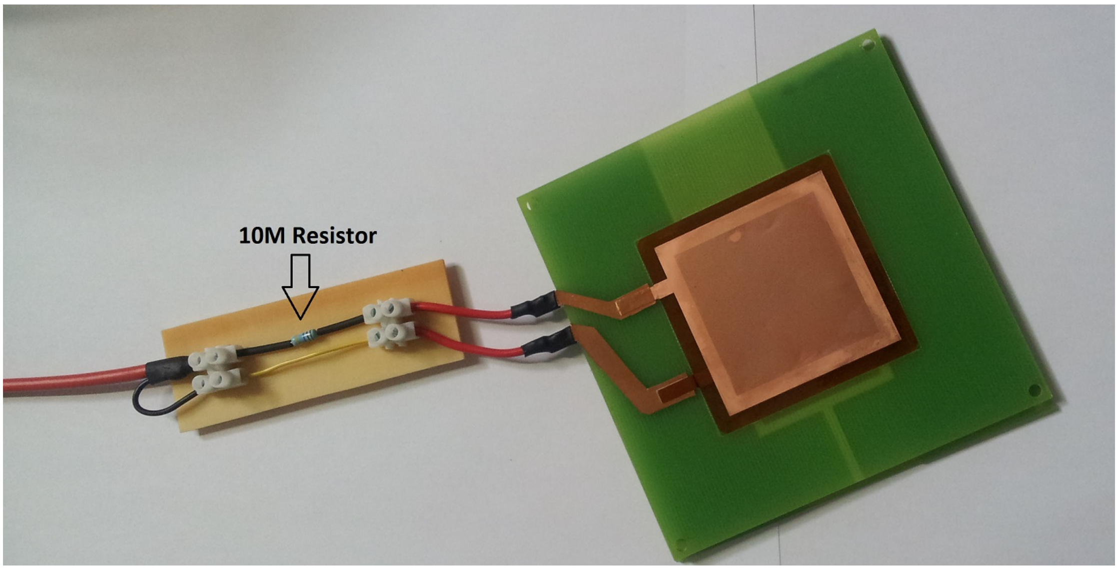


**Figure 4.22.:** Setup to test each GEM at high voltages and to burn away impurities

To test the device itself, we again performed a measurement with the well-known $ArCO_2$, which now showed events even without putting a source on the detector. After disassembling the device once more, each foil was cleaned with pure oxygen and connected to a high voltage to burn possible dust-particles away. The top layer of the GEM was connected to a 10 M$\Omega$ resistor, the bottom layer directly to ground. The whole setup can be seen in fig. 4.22. We then applied a voltage of up to 500 V on each GEM (in the detector the voltage does not exceed 400 V). With this setup we observed each foil for about 20 minutes, where we could see several sparks on the foils in the first few minutes, so some dust got burnt off. After about 10 minutes, the number of sparks decreased to about 1. . . 2 over the remaining 10 minutes.
Once everything was put back together, the unwanted events without source were gone. Since helium still had discharges even at voltages barely above 150 V, it seems that helium has only a very narrow range of voltages where it can be operated safely.

Our final goal, however, was to use pure hydrogen, so we decided to not ascertain the optimal voltage-range in helium and instead focus on other pure gases.

### 4.3.2. Argon

Before coming to the argon measurements, let me shortly review the voltage assignment: In the detector, there are 7 different regions, 6 of them, $V_1$ to $V_6$ in fig. 3.3, from the drift cathode to the bottom of the third GEM having the same voltage, and the seventh, $V_7$ below the third GEM, with a different voltage. The first measurement with pure argon was performed at a voltage of 333V/620V, where some events could be seen just above the noise-threshold. We didn't want to apply a higher voltage without first making sure we had a stable setup. With this voltage, a first 1-hour measurement was done, which can be seen in fig. 4.23.
In this measurement we have only few events because of the low voltage, which leads to a lower gain. It is also noticeable that in channel 11 there are a lot more events compared to the other channels. This could once again be a problem with impurities in the chamber, so we evacuated the chamber over 3 days to make sure that most of the other gases like oxygen or $H_2O$ are removed. After the chamber was cleaned, a first test measurement went well, so we decided to try some measurements with different pressures inside the chamber. At first, the pressure was lowered to about 0.7 bar. For that, the gas has to stay inside the detector and can not, as before, be flushed through. The idea behind this is, that with lower pressure the gas inside the chamber is less dense and therefore the incident electrons have a longer free mean path and will be accelerated more, which allows for higher gain at lower voltage between the GEM foils. The problem is, that the voltage has to be adjusted to the pressure, but with lower pressure the discharges already started at a voltage of 280 V in between the GEMs, which might be caused by gas leaking into the detector volume. With such a low voltage it was impossible to see any events.
After that we increased the pressure to 1.2 bar, which allowed us to use higher voltages. With this pressure it was possible to perform a 90 min measurement without any discharges at voltages of 357V/620V. The measurement can be seen in fig. 4.24. In this measurement one can see a high amplification due to the fact that there are still a lot of signals above the high threshold of our discriminator at 4 V.
After this measurement, we performed the already explained experiment with the $^{55}$Fe-source inside the detector which needs mentioning here because this caused a problem in the following measurement. After the $^{55}$Fe-source was removed, we wanted to do one more measurement with pure argon. Once more the pressure was adjusted to 1.2 bar and the voltage to 357V/620V, so the conditions were the same as before. But now there were large fluctuations in the event rate. In time-periods of 2 to 5 minutes, the rate changed from about 10 Hz to over 100 Hz and back. Since the only thing that changed from the previous measurement to now was the 4. kapton-foil inserted

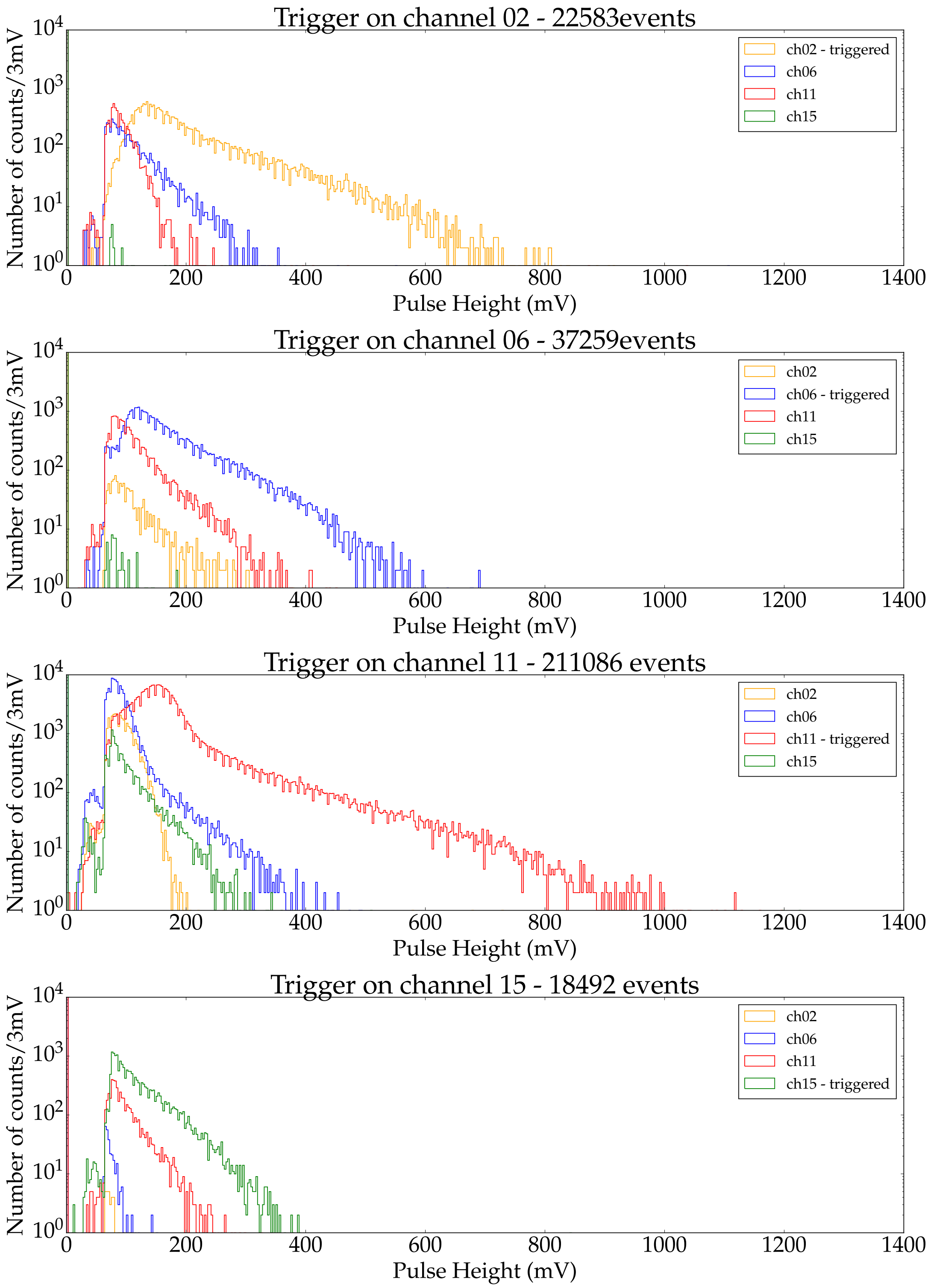


**Figure 4.23.:** First 60 min. measurement with pure argon at 333V/620V and 1 bar, still with a lot of noise. Trigger problems in ch. 11 and different amplifications in all channels.

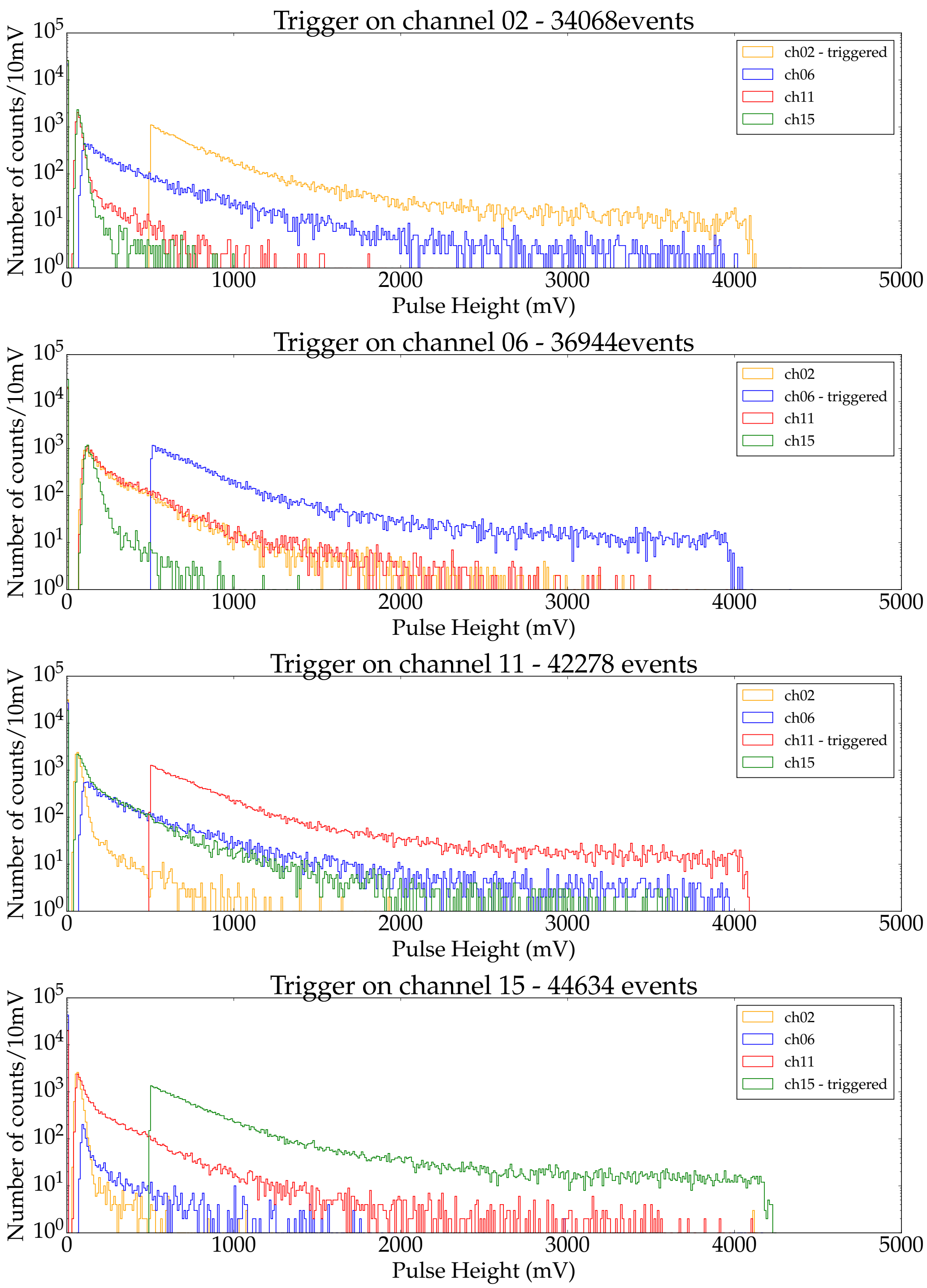


**Figure 4.24.:** Argon measurement at 357V/620V and 1.2 bar. Measurement over 90 min. High gain up to max. channel indicates higher amplification as for the $ArCO_2$ measurements. The discriminator has an upper threshold at about 4 V, which is the reason for this sharp cut at around 4 V.

to put the $^{55}$Fe-source on top, the reason for this fluctuation most likely comes from this foil. One possible explanation is, that the foil charges up over time and after a few minutes all charges are released. After removing the foil again, the fluctuations were gone, as confirmed by another measurement.
One last argon measurement was done over night, starting at about 4 pm. The measurement went well until about 8:30 pm, when discharges started, persisting through the night until 9 am in the morning. A 2-hour part of one channel of this discharge-measurements is compared to 4 hours of actual measurement in the same channel in fig. 4.25. The voltage was not changed from one measurement to the other. In the discharge-case, no channel is identifiable as trigger anymore, since all channels get high signals all the time. It is also notable that even in the highest possible channel 8096 of the ADC, corresponding to 8.1 V, a lot of signals are present, so overflow-signals get stored and are shown in the highest possible channel.

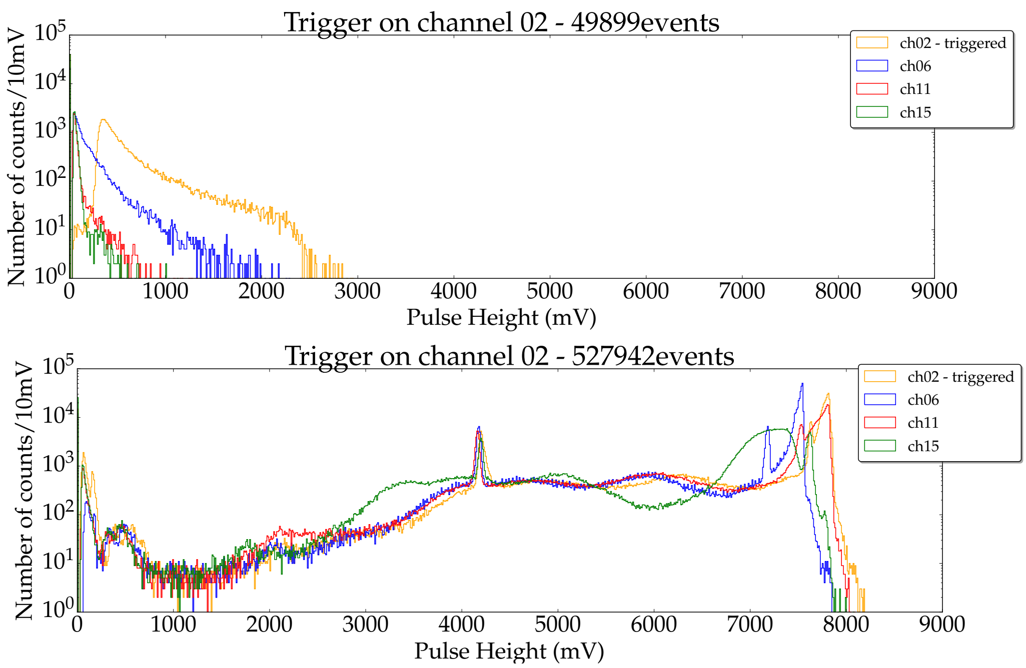


**Figure 4.25.:** Actual events in one channel over 4 hours (top) compared to discharges over two hours (bottom) with the same voltages in the same channel

After these discharges, we had to check all GEM foils as well as the cathode and anode for damage. For that, we had a look at the GEM foils under the microscope, where we could find some small pollution as well as a few damaged holes (see 4.26), but since these are just in the $\mu$m region and there are only very few of them, it shouldn't affect the measurements. The left picture shows an impurity on the foil, which could be soldering tin, while on the right side one can see damage done by the discharges,

destroying the copper-layer next to the holes.
After examining the GEMs under the microscope, we once again used the method explained before to clean the foils by connecting them directly to a high voltage via a 10 MΩ resistor, to see how stable each GEM is to discharges. For each GEM, we could reach at least 550 V with only 2...5 sparks over 20 min. each.

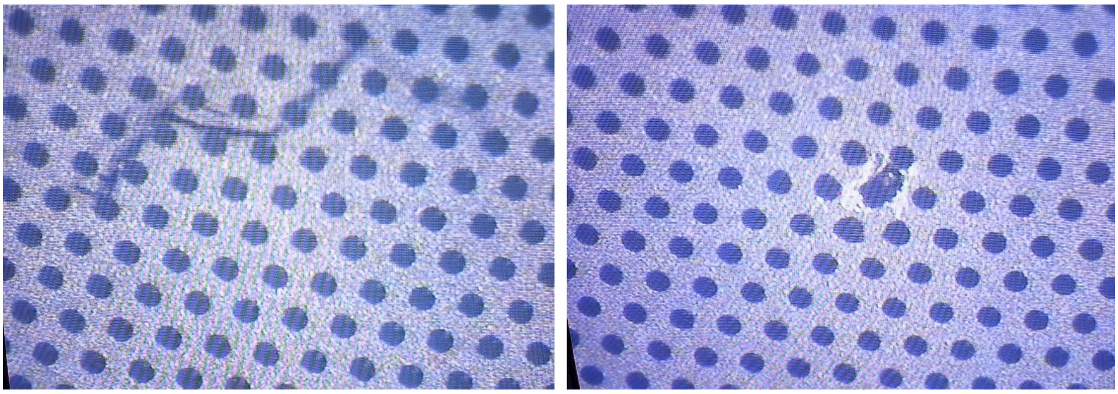

**Figure 4.26.:** Microscope pictures of impurities (left) and damage on the GEM foils (right)

After the GEMs were tested and considered operable, we decided to exchange the cathode, since the aluminized Mylar foil of the old cathode already looked battered from the constant dis- and reassembling of the detector. The new foil can be seen in fig. 4.27.

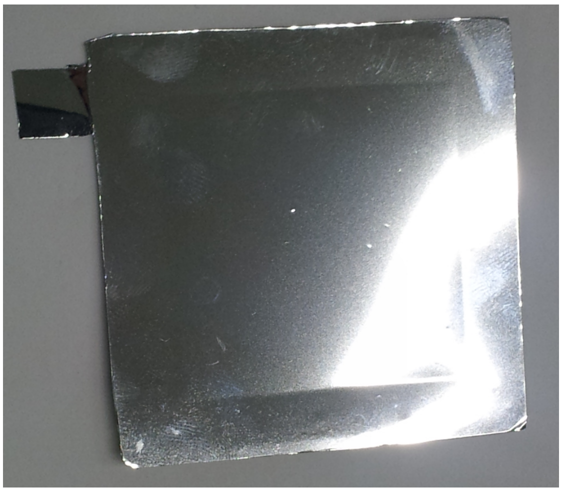

**Figure 4.27.:** The new cathode, stretched and glued to a new frame

To assemble the foil, it has to be stretched with the same device shown and explained

in section 3.1. Once the foil is stretched, the new frame can be glued on the foil and, after the glue has dried, the finished cathode can be cut out of the foil and reassembled to the detector. To test this new setup, we changed the gas to the well-known $ArCO_2$ again to make sure we can see events at the previously used 347V/670V.
After it was confirmed that there were no problems, one last measurement with pure argon was performed: After flushing the whole device 3 times with argon to make sure it is as clean as possible, we put in 1 bar of argon and let it stay inside the detector without flushing. With this method it was possible to see events at 317V/500V, which we then used to do a 2-hour-measurement, as shown in fig. 4.28 for one of the channels. This time the measurement was stable over the whole two hours. In this measurement we could reach a similar gain as for $ArCO_2$ shown in fig. 4.18, but at a much lower voltage.

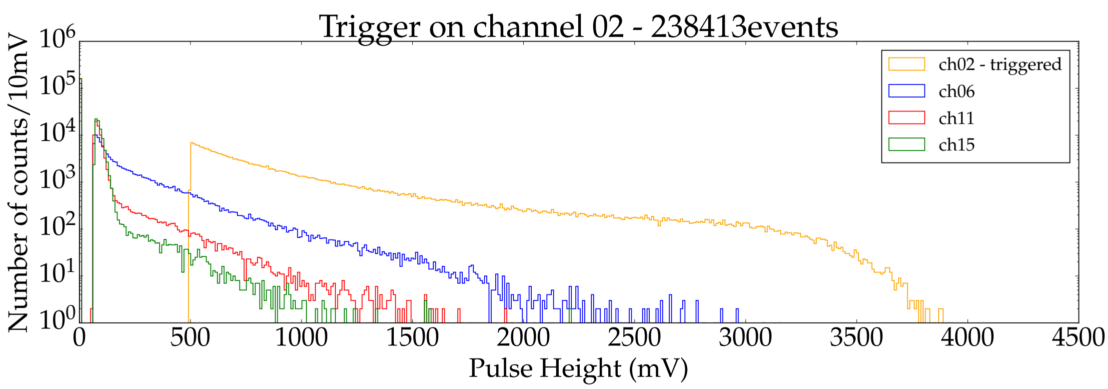


**Figure 4.28.:** Channel 2 of pure argon measurement at 317V/500V over 2 hours

## 4.3.3. Neon

As a last noble gas we started measuring neon, which turned out to require much lower voltages than the other gases up to now. A first test showed events for voltages of 192V/300V. The gain for such low voltages is not very high, but over a time of 10 hours we could get about 15000 events per readout-pixel. One of the channels is shown in fig. 4.29, the others can be found in appendix C. Unfortunately, in this measurement there were once again problems with the trigger in one of the channels (channel 6), so this measurement had to be excluded and is not shown in the appendix. Because of the low voltage, there are no signals higher than about 1000 mV, so we slowly raised the voltage and performed another measurement at 208V/400V.
With this setup we had a raise of gain due to the higher voltage compared to our first measurement with neon by a factor of two. The second measurement can be seen in fig. 4.30 (Note the different voltage-range on the x-axis).

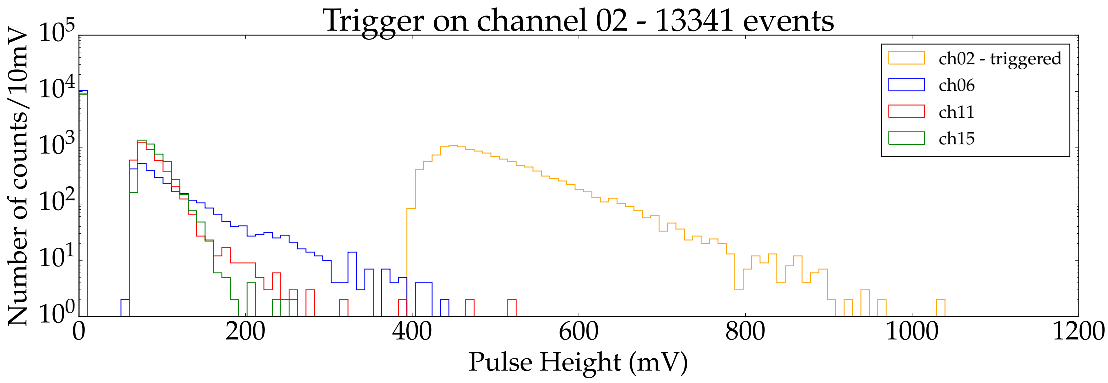


**Figure 4.29.:** Channel 2 measurement of pure neon at 192V/300V over 10 hours. Note the low gain and amplification. Only events up to 1000 mV can be seen.

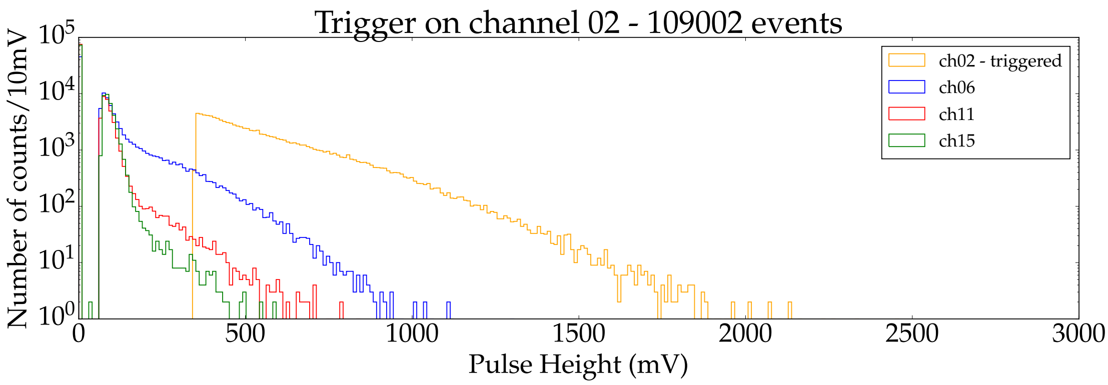


**Figure 4.30.:** Channel 2 measurement of pure neon at 208V/400V over 4 hours. Double gain and amplification compared to fig. 4.29.

The third and last measurement with neon was done at 225V/450V where we could once again expect an increase in the rate and gain. This last measurement is shown in fig. 4.31 and notably, over 30 minutes the total number of events on channel 2 is 128,000, and the average on all 4 channels is 131,000 events per channel.
So now we have a rate of 80 Hz, again a factor of 10 more than the previous measurement, as well as a higher gain, since now there are events up to 4000 mV comparable to our $ArCO_2$-measurement.

### 4.3.4. Hydrogen

After we were able to measure some pure gases (argon, neon), we decided to go one step further and test the setup with pure hydrogen, which is the gas used in active-

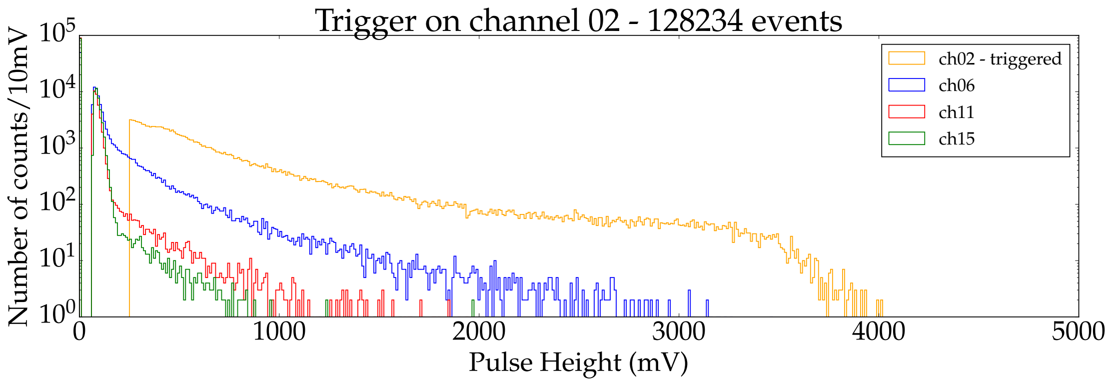


**Figure 4.31.:** Channel 2 measurement of pure neon at 225V/450V over 30 minutes. Double amplification compared to fig. 4.30.

target GEM-TPCs. It turned out, that we had to go to much higher voltages than with any other gas measured previously. The first events could be seen at voltages of about 433V/400V, so we performed a first measurement with that voltage. Again, we first evacuated the chamber and then flushed it 3 times with pure hydrogen, before finally filling it with hydrogen to a pressure of 1 bar and letting this hydrogen stay in the detector without continuously flushing.
In this first measurement we had to stay at an upper voltage of 3000 V on the anode, corresponding to a voltage of 433 V in each GEM-region, since our HV Power Supply (NHQ 203M) has a maximum output voltage of 3000 V. In this first measurement, which was done over 100 min., we had a rate of 8 Hz for all channels together. The gain in this measurement was low compared to other gases, considering the high voltage applied. The results of this measurement can be seen in fig. 4.32. Again, the trigger levels were not all the same. While channel 2 and 15 had the trigger at 200 mV, channel 6 was set to 80 mV and channel 11 to 240 mV. This issue was addressed in the next measurement, as well as a change of the power supply, where we wanted to use a new "iseg THQ 3CH 2HE 100W", which is able to deliver up to 6 kV in one channel. Unfortunately this device was broken since it couldn't deliver a stable voltage, so we had to go back to an old "Oltronix A3, 6K" power supply. In our next measurement we used a voltage of 458V/500V, so we had events that were clearly distinguishable from noise (see fig. 4.33). The first picture shows the signals directly after the preamplifier, while the second picture shows the shaped signal after the shaping- and spectroscopy amplifier. One can see that the trigger is set in such a way that it overlays the signal peak together with a few microseconds before and after the peak. Notice also the difference in peak height (different mV/div) as well as the different signal length in the upper and lower picture.
These events were recorded over 150 minutes and can be seen in fig. 4.34. With

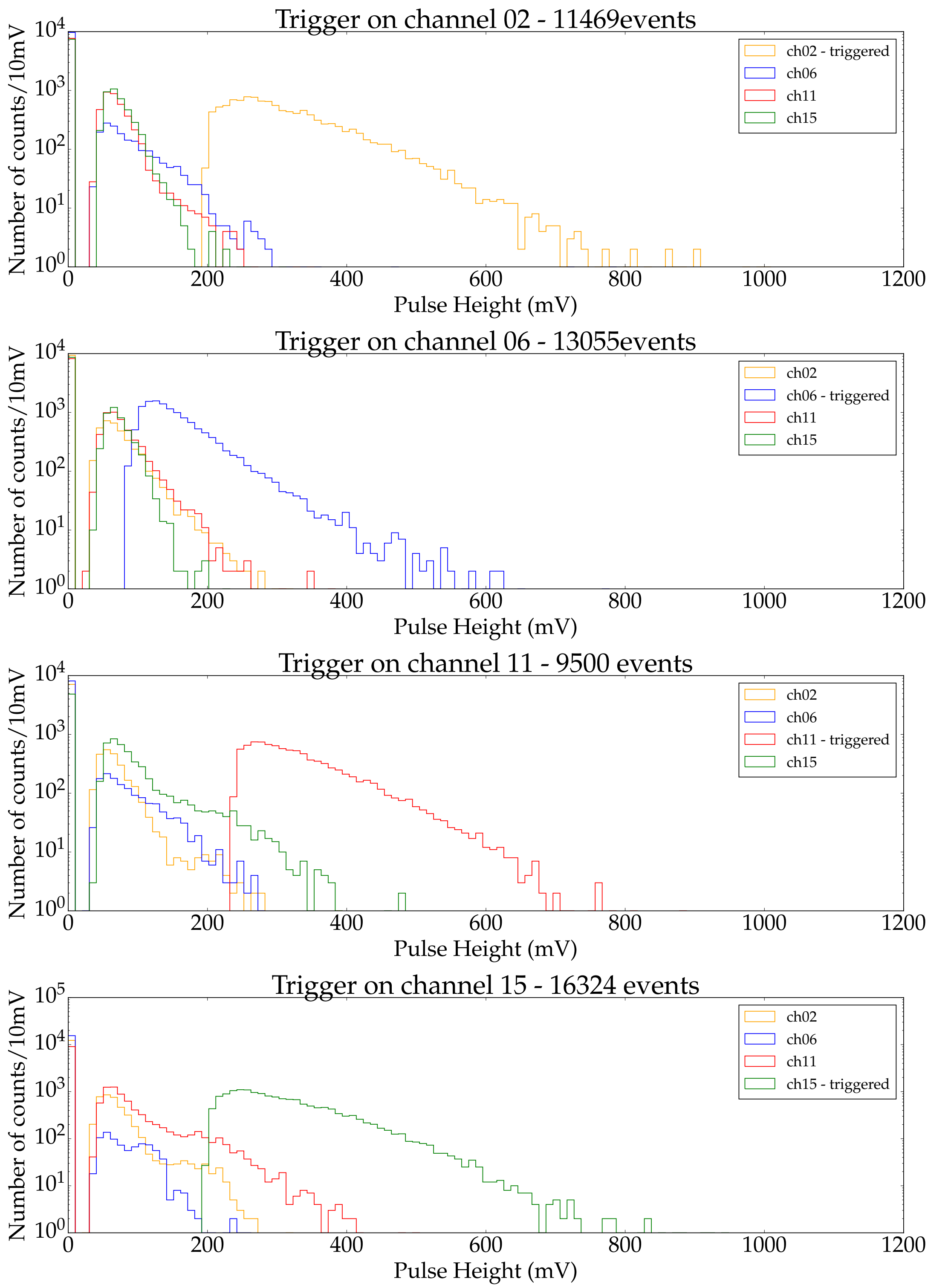


**Figure 4.32.:** Measurements of pure hydrogen at a voltage of 433V/400V over 100 min (rate: 8 Hz). Low gain despite high voltage compared to other gases

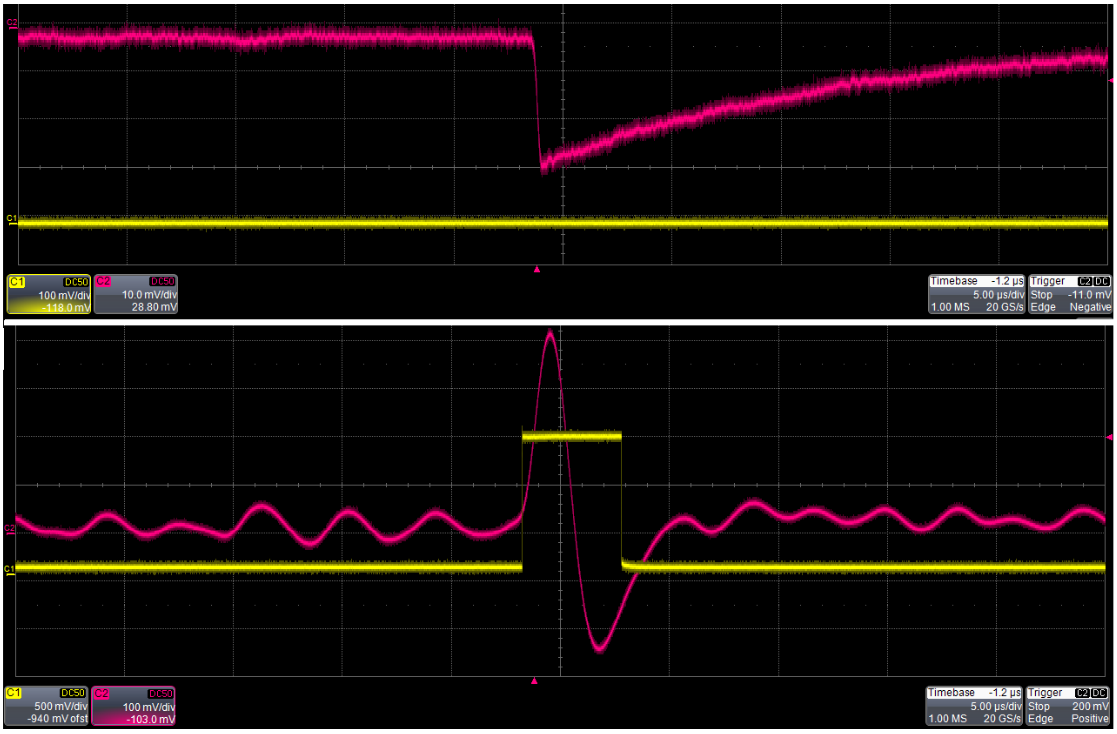


**Figure 4.33.:** First measured H2 events at voltage of 458V/500V. Top picture shows signal after preamplifier, bottom picture after spect. amplifier where also the yellow trigger is seen, overlaying the signal. Top picture has 10 mV/div y-axis, bottom picture 100 mV/div for the signal. Time base was the same for both measurements.

this higher voltage, the amplification was again much higher than in the previous measurement, so signals up to 3000 mV could be seen. Although we used such a high voltage, the gain was still lower compared to the 4000 mV of $ArCO_2$.
With this measurement we confirmed that, on one hand, a much higher voltage is needed for hydrogen than for other pure gases, while on the other hand the setup also was running stable at high voltages. With these measurements we get an important set of data which is necessary for designing an active target GEM-TPC.

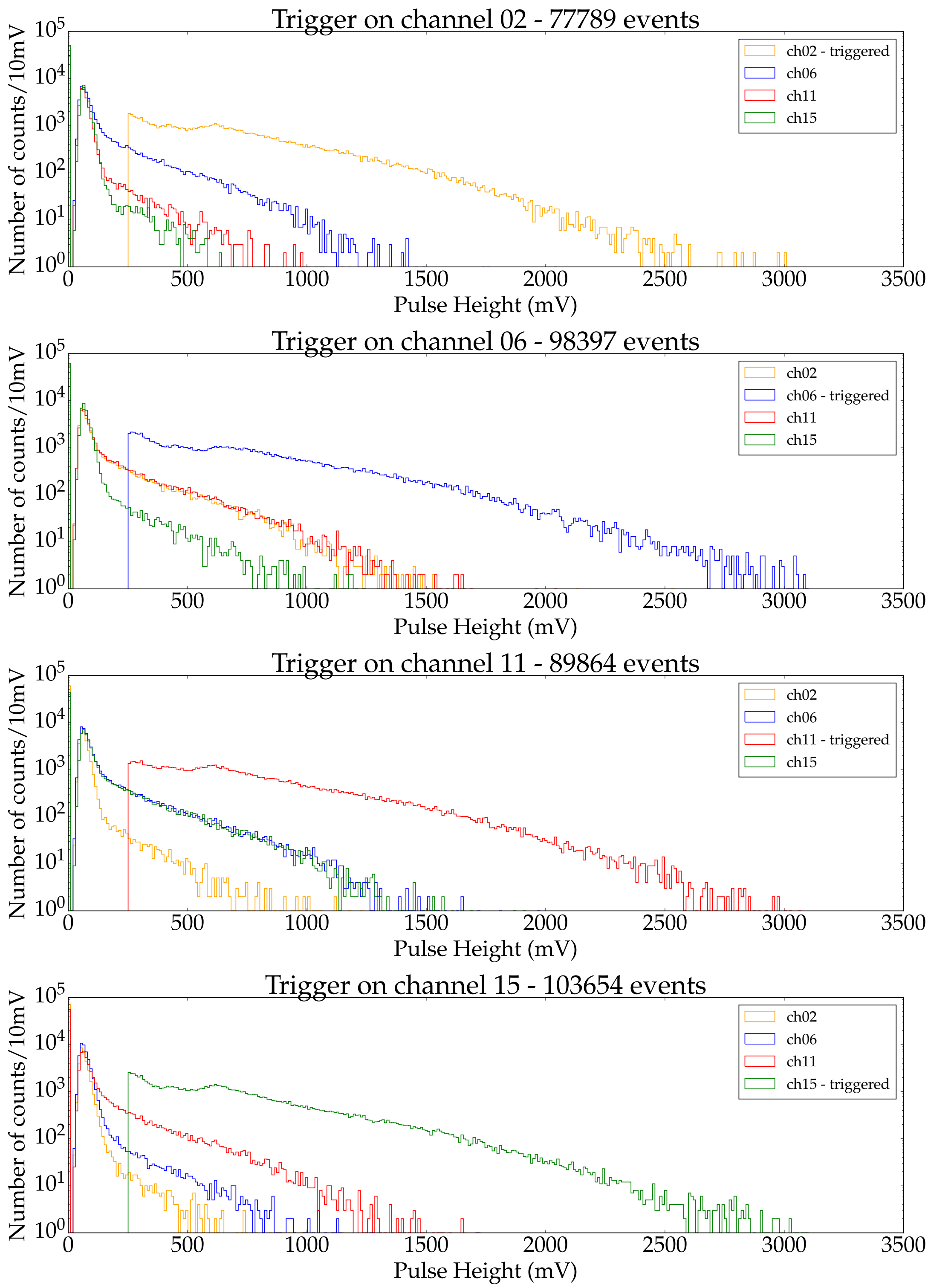


**Figure 4.34.:** Measurements of pure hydrogen at a voltage of 458V/500V over 150 min. (rate: 41 Hz). Much higher gain compared to fig. 4.32 because of higher voltage

# 5. Conclusion

The goal of this thesis was to study the performance of a triple-GEM detector. To start with, the detector had to be tested and a measurement chain to read out the data had to be established. Once the setup was complete, the first step was to perform measurements in a stable $ArCO_2$-environment. Different readout-channels have been compared with each other to ensure well-known settings for the next measurements. Once the short- and long-term stability of the detector has been confirmed by comparing different runs on the same channel, the next step was to determine the gain of the detector. To do that, a $^{55}$Fe-source producing X-rays with an energy of around 6 keV was placed on top of the detector, so the deposited charge in the pixel-anode could be used to directly calculate the number of collected electrons. With this method, the gas-gain of the triple-GEM detector was determined to be about 10,000, at voltages of 373V/620V in $ArCO_2$, corresponding to a multiplication factor of about 20 per GEM. The focus was to study the detector, especially with pure gases. Several measurements with pure argon, neon and hydrogen delivered results that can be compared with each other, determining a set of data for amplification under stable operation. These values turned out to be very different for the three gases: While neon already shows signals at a voltage of 192V/300V, argon needs a voltage of at least 300V/500V to measure events in the readout-anode. Hydrogen, again, needs a still higher voltage of at least 433V/400V to get first signals but is also very stable at these high voltages. The hydrogen measurement is of special significance, since to this day there are only very few measurements of triple-GEM detectors with pure hydrogen available.

The overall goal of understanding the setup and operation of a triple-GEM detector with pure gases has therefore been achieved. The data deliver a valuable input for further design studies of an active target GEM-TPC.

# A. Setup

In this appendix, the voltage divider for the triple-GEM can be seen in fig. A.1. As one can see, the HV-supply is connected to the drift-anode via a 10 MΩ resistor, while in between each of the different voltage-regions there is a total resistance of 23 MΩ. This ensures the same voltage in all 6 regions from the "Drift-to-GEM1TOP" to the "GEM3TOP-to-GEM3BOT" region. The GEM3BOT is then connected to another transfer-voltage, so the voltage after that, between GEM3BOT and cathode can be adjusted separately.

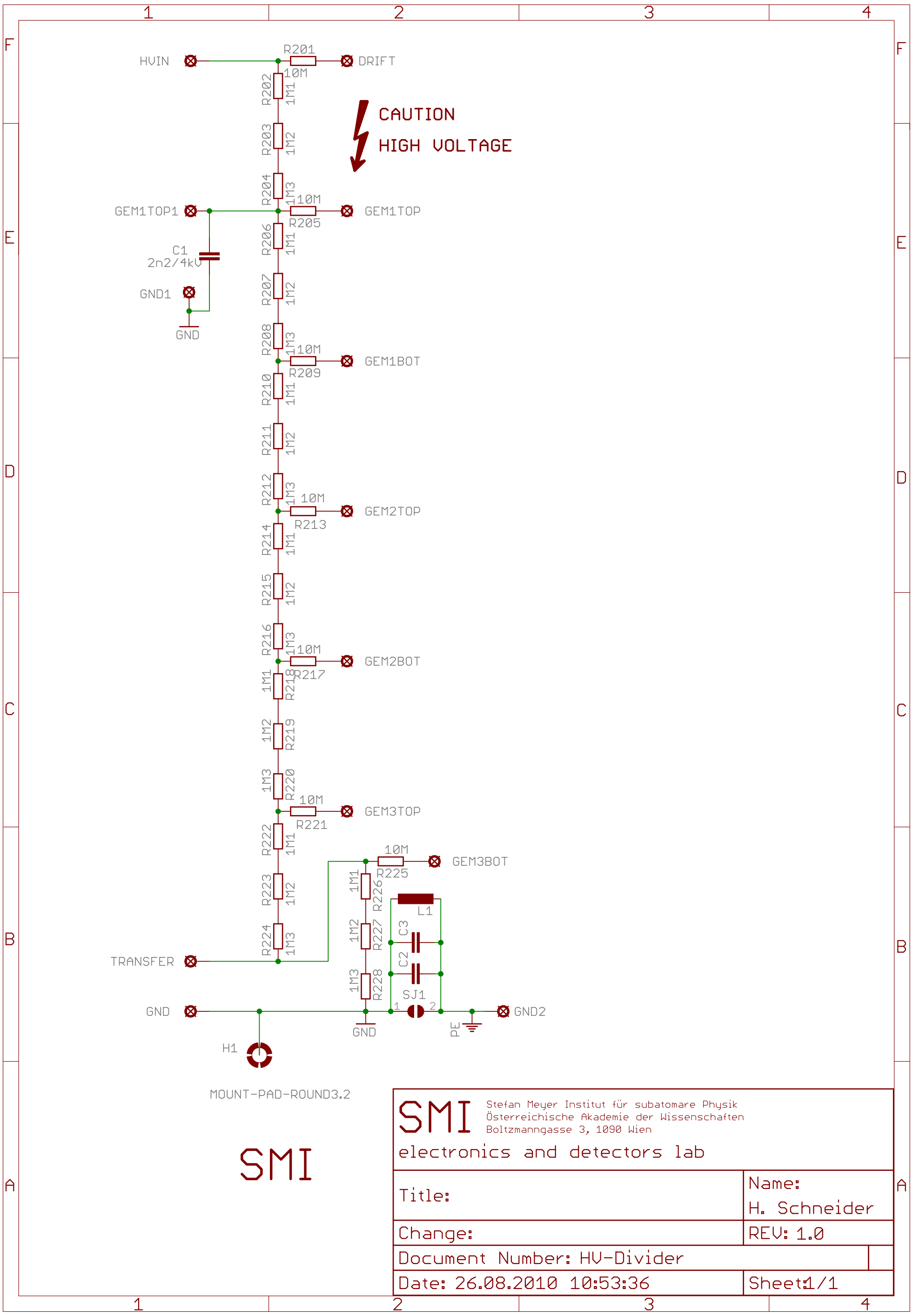


**Figure A.1.:** Voltage divider

# B. Data $ArCO_2$ measurements

## B.1. Measurements ch. 1 to 16

In this appendix, the measurements for all channels, 1 to 16, are depicted. Each channel was measured over several 2 hour runs.

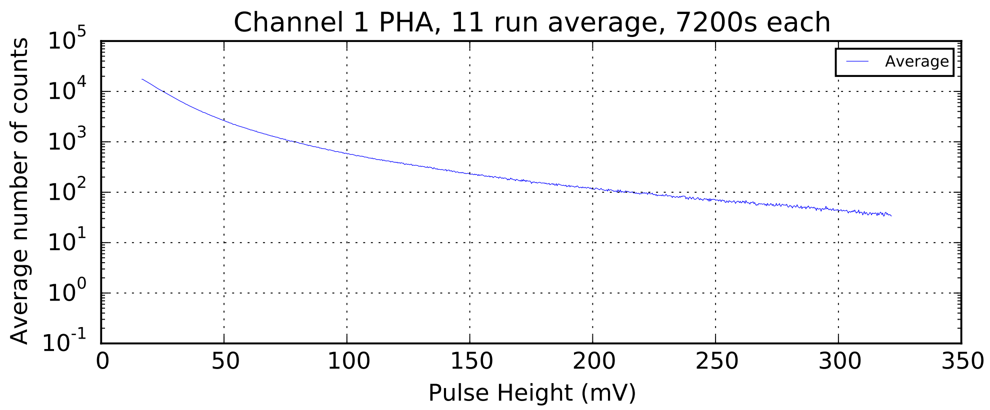


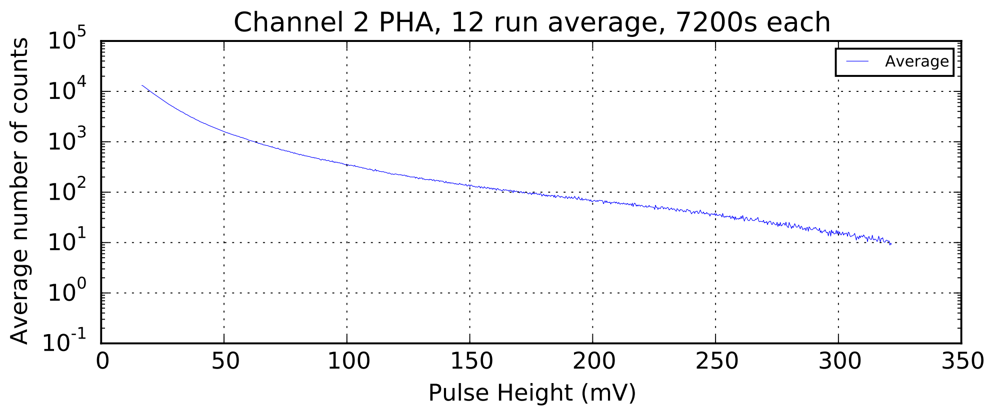

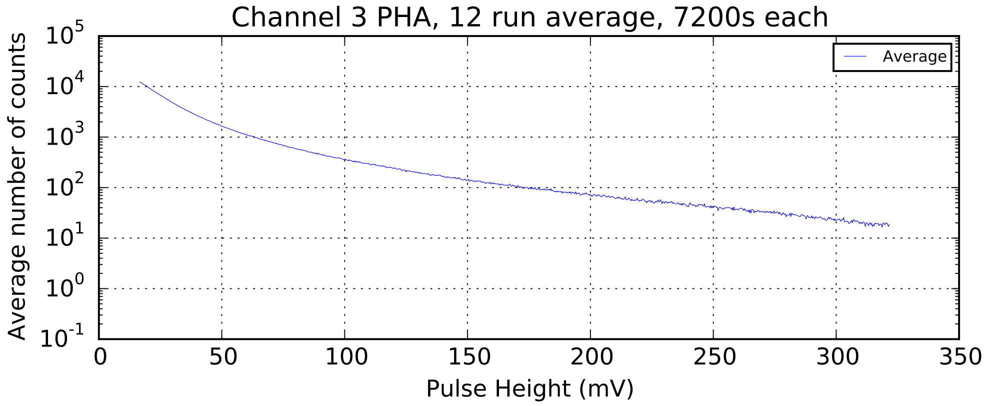
Channel 3 PHA, 12 run average, 7200s each
Average
Average number of counts
Pulse Height (mV)
0
50
100
150
200
250
300
350
10^5
10^4
10^3
10^2
10^1
10^0
10^-1

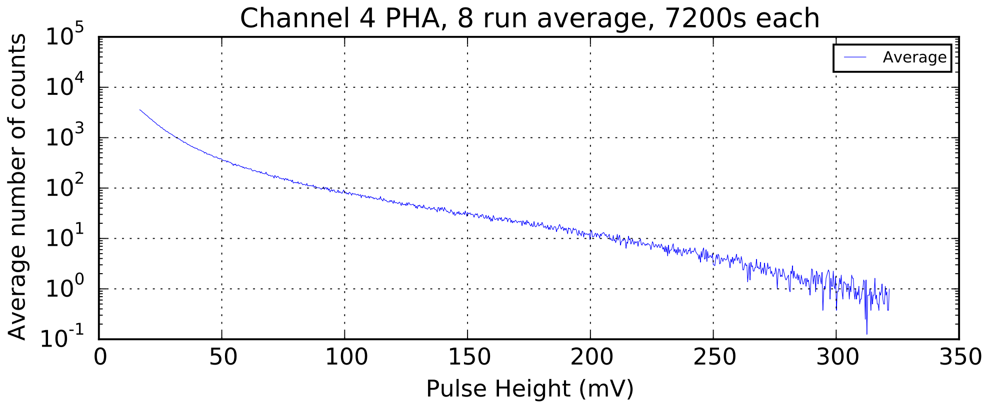
Channel 4 PHA, 8 run average, 7200s each
Average
Average number of counts
Pulse Height (mV)
0
50
100
150
200
250
300
350
10^5
10^4
10^3
10^2
10^1
10^0
10^-1

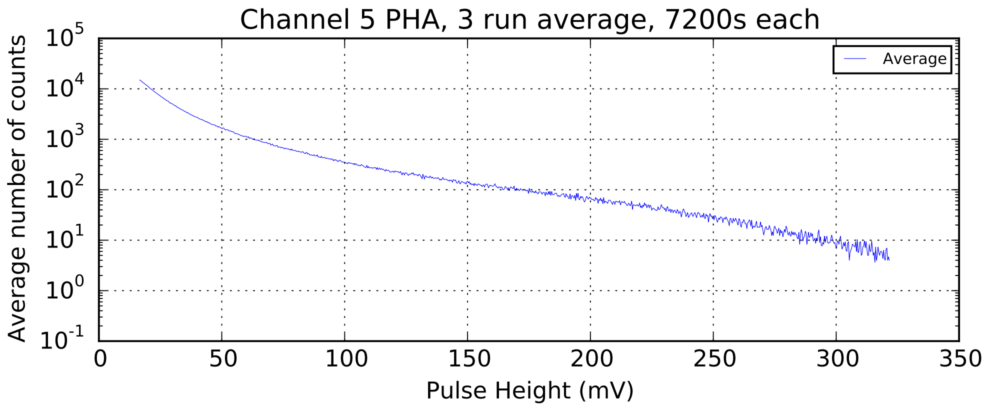
Channel 5 PHA, 3 run average, 7200s each
Average
Average number of counts
Pulse Height (mV)
0
50
100
150
200
250
300
350
10^5
10^4
10^3
10^2
10^1
10^0
10^-1

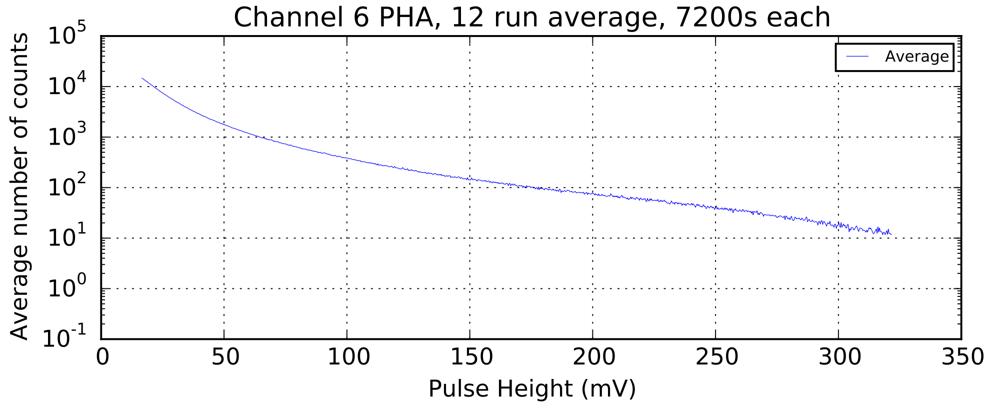
Channel 6 PHA, 12 run average, 7200s each
Average
Average number of counts
Pulse Height (mV)

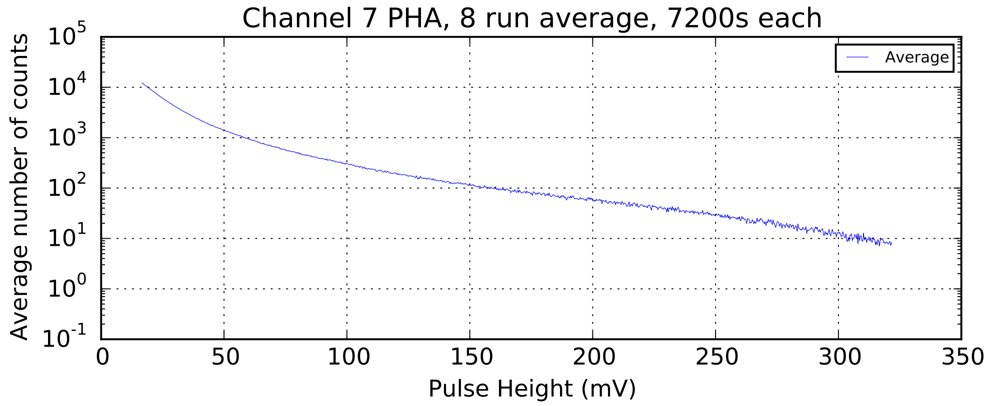
Channel 7 PHA, 8 run average, 7200s each
Average
Average number of counts
Pulse Height (mV)

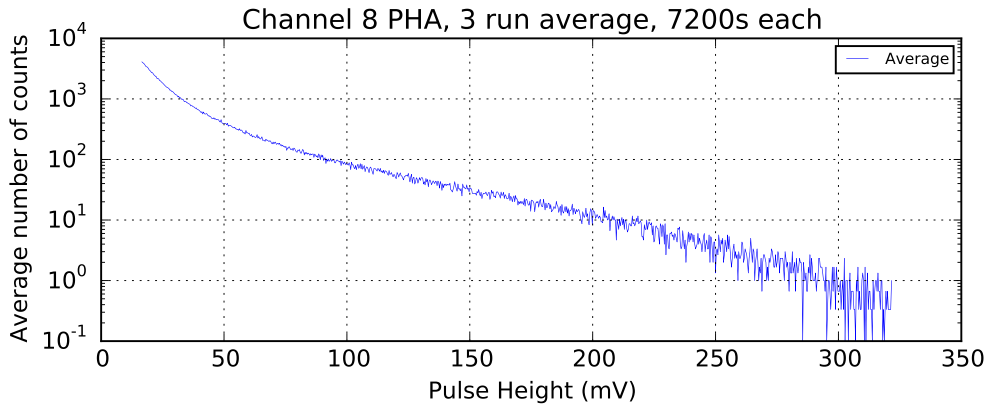
Channel 8 PHA, 3 run average, 7200s each
Average
Average number of counts
Pulse Height (mV)

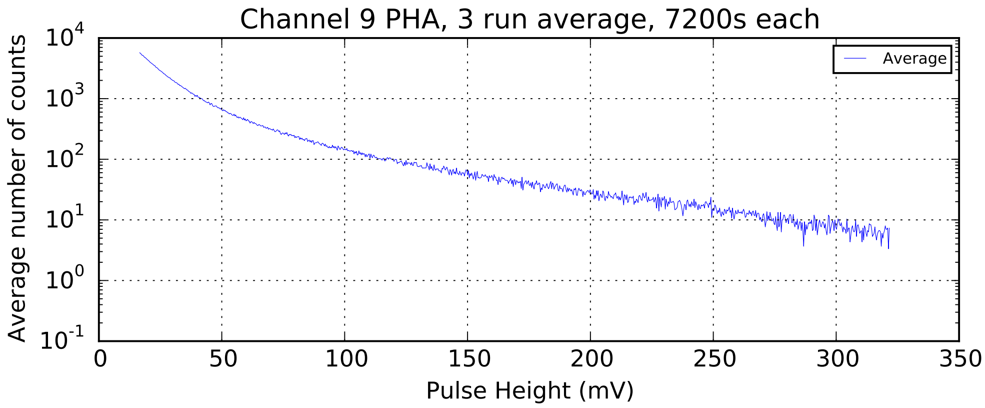
Channel 9 PHA, 3 run average, 7200s each
Average
Average number of counts
$10^{4}$
$10^{3}$
$10^{2}$
$10^{1}$
$10^{0}$
$10^{-1}$
0
50
100
150
200
250
300
350
Pulse Height (mV)

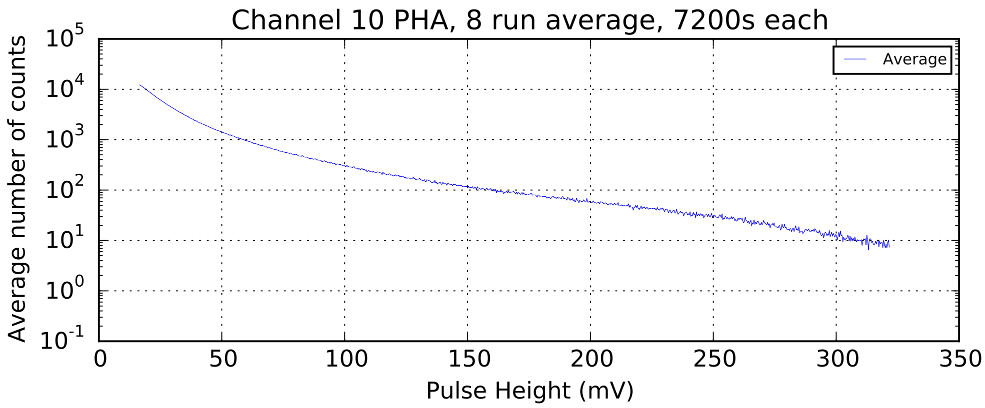
Channel 10 PHA, 8 run average, 7200s each
Average
Average number of counts
$10^{5}$
$10^{4}$
$10^{3}$
$10^{2}$
$10^{1}$
$10^{0}$
$10^{-1}$
0
50
100
150
200
250
300
350
Pulse Height (mV)

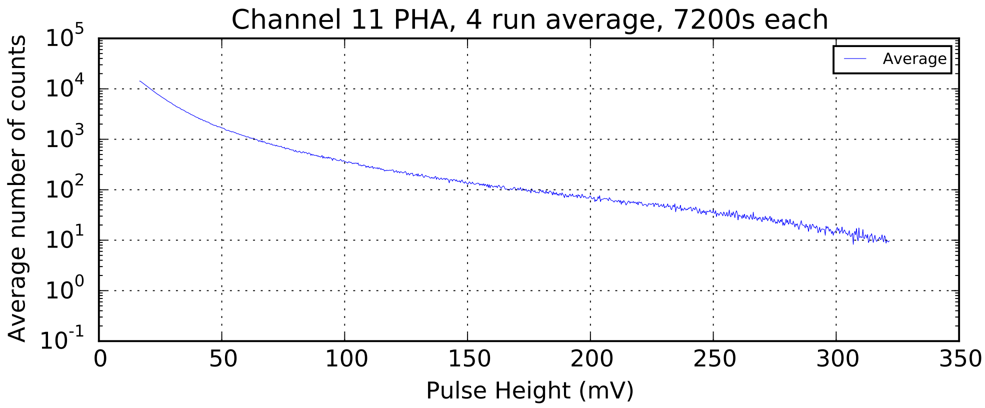
Channel 11 PHA, 4 run average, 7200s each
Average
Average number of counts
$10^{5}$
$10^{4}$
$10^{3}$
$10^{2}$
$10^{1}$
$10^{0}$
$10^{-1}$
0
50
100
150
200
250
300
350
Pulse Height (mV)

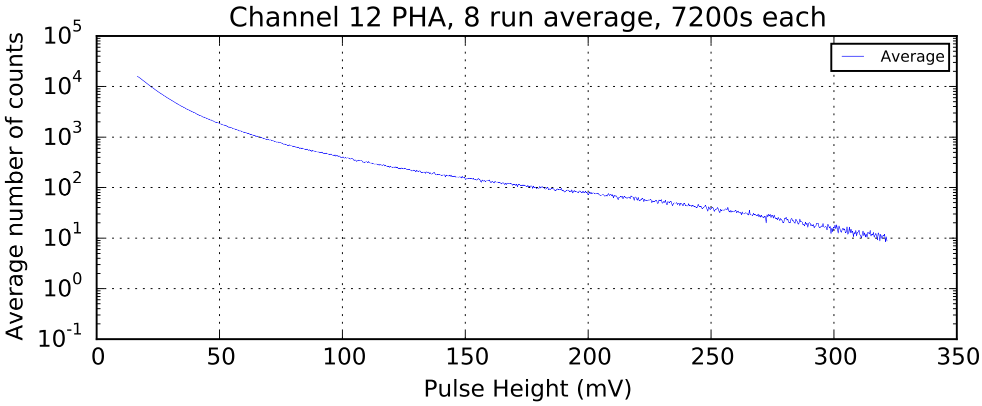
Channel 12 PHA, 8 run average, 7200s each
Average
Average number of counts
10^5
10^4
10^3
10^2
10^1
10^0
10^-1
0
50
100
150
200
250
300
350
Pulse Height (mV)

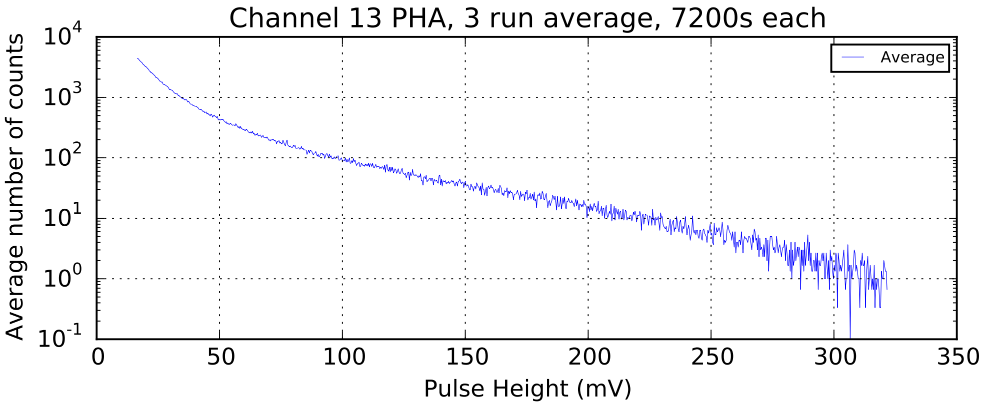
Channel 13 PHA, 3 run average, 7200s each
Average
Average number of counts
10^4
10^3
10^2
10^1
10^0
10^-1
0
50
100
150
200
250
300
350
Pulse Height (mV)

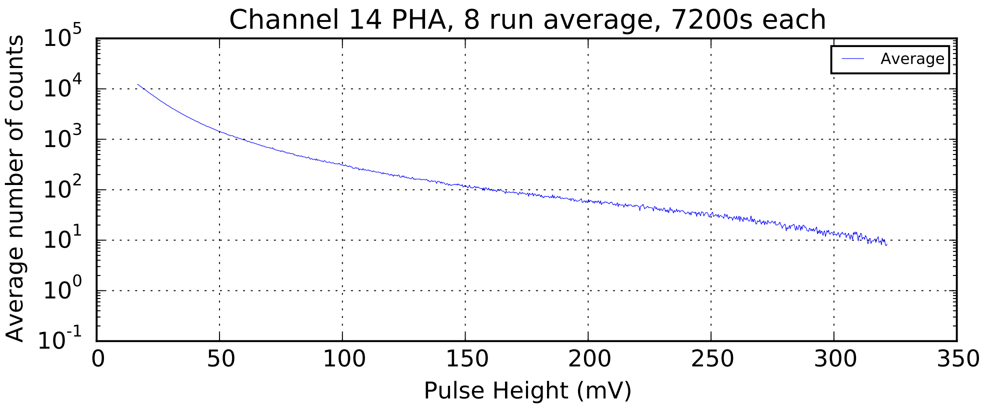
Channel 14 PHA, 8 run average, 7200s each
Average
Average number of counts
10^5
10^4
10^3
10^2
10^1
10^0
10^-1
0
50
100
150
200
250
300
350
Pulse Height (mV)

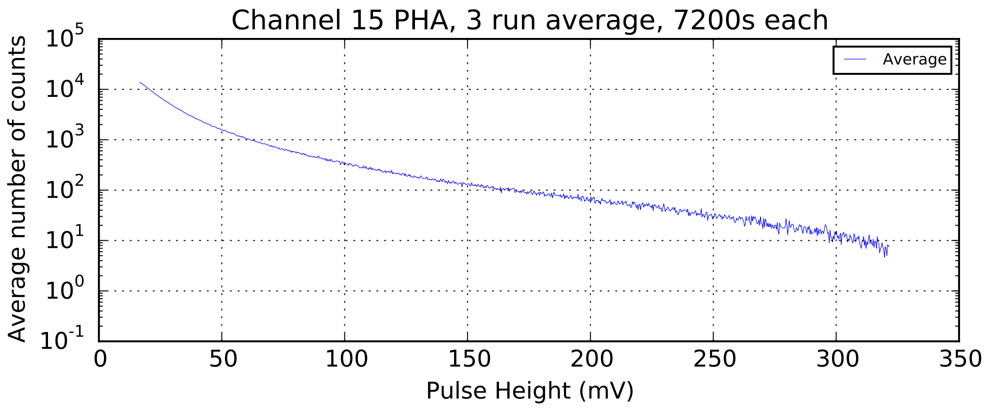


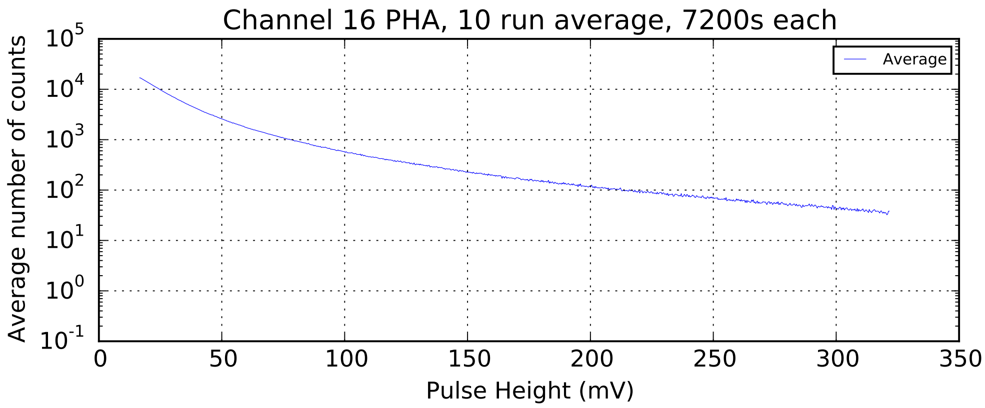


## B.2. Short term stability

In this appendix, the short term stability of channel 2 is depicted both over the whole spectrum from 0 mV to 350 mV as well as several zoomed in versions.

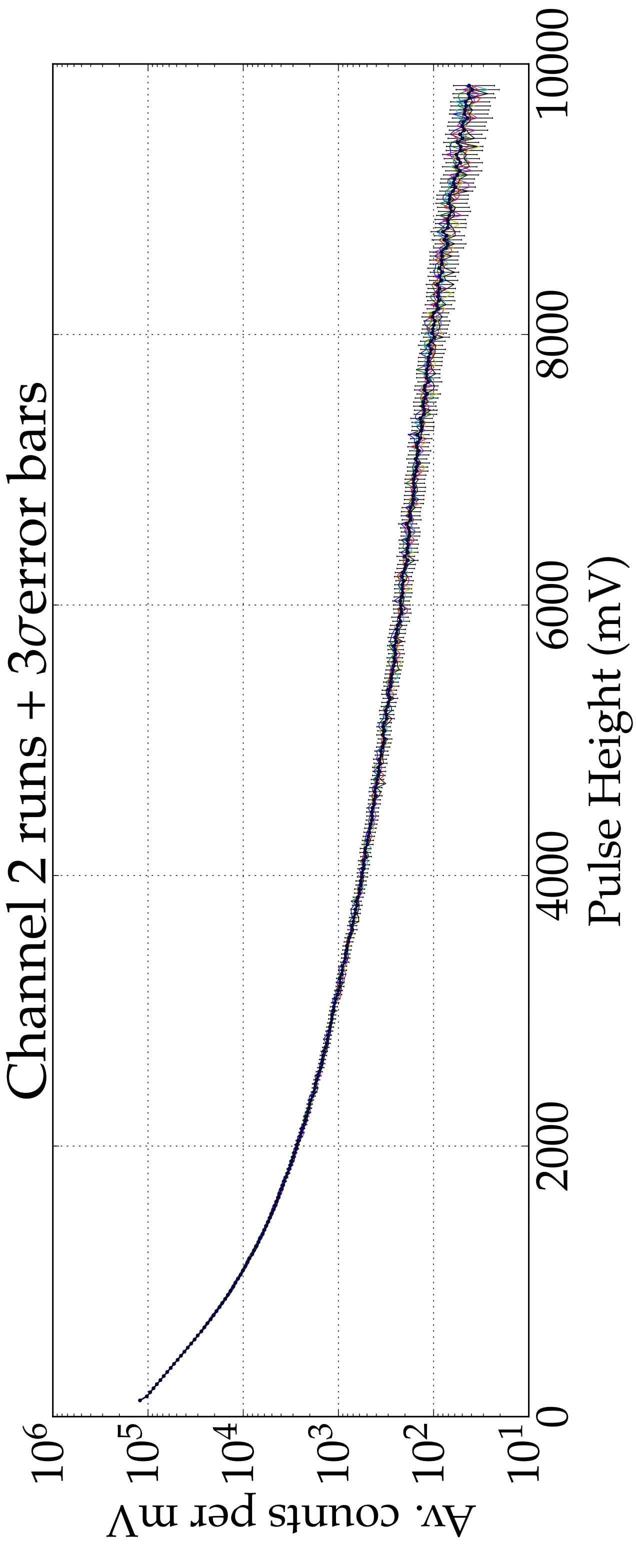
Channel 2 runs + 3σerror bars
Av. counts per mV
Pulse Height (mV)
10^6
10^5
10^4
10^3
10^2
10^1
0
2000
4000
6000
8000
10000

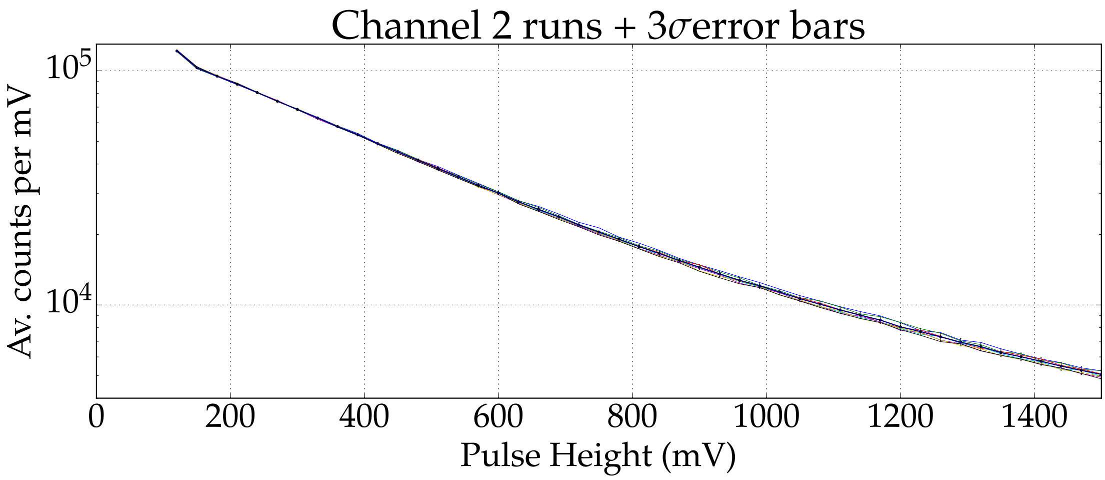
Channel 2 runs + 3σerror bars
10^5
10^4
Av. counts per mV
0
200
400
600
800
1000
1200
1400
Pulse Height (mV)

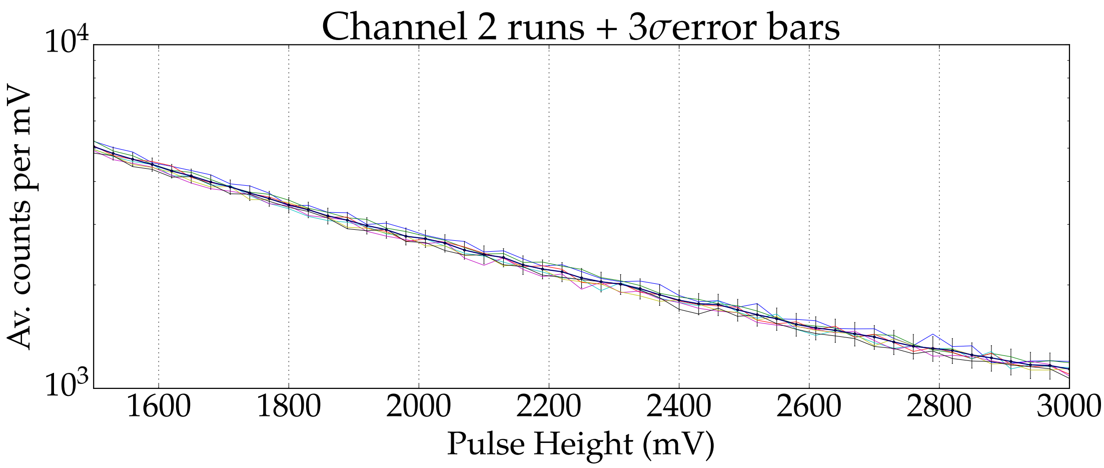
Channel 2 runs + 3σerror bars
10^4
10^3
Av. counts per mV
1600
1800
2000
2200
2400
2600
2800
3000
Pulse Height (mV)

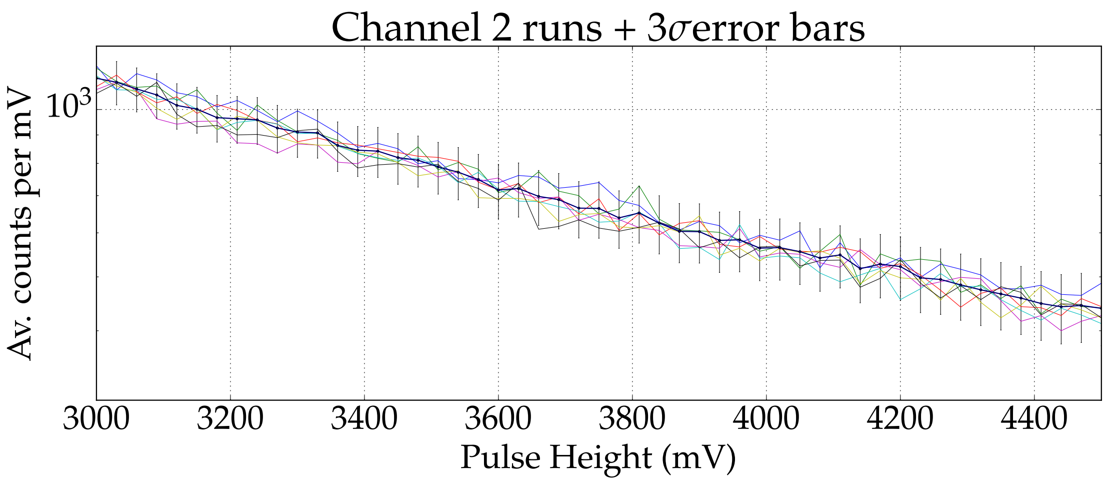
Channel 2 runs + 3σerror bars
10^3
Av. counts per mV
3000
3200
3400
3600
3800
4000
4200
4400
Pulse Height (mV)

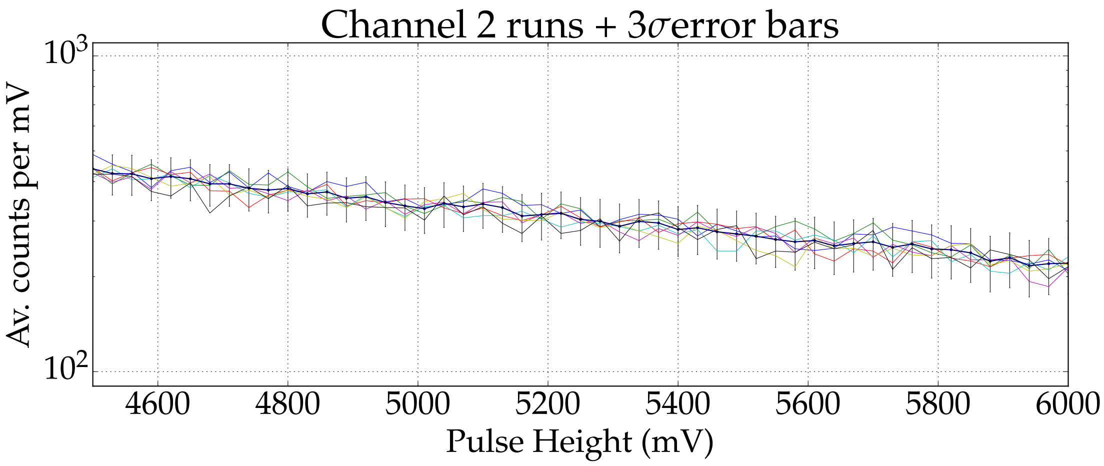
Channel 2 runs + 3σerror bars
Av. counts per mV
$10^3$
$10^2$
4600
4800
5000
5200
5400
5600
5800
6000
Pulse Height (mV)

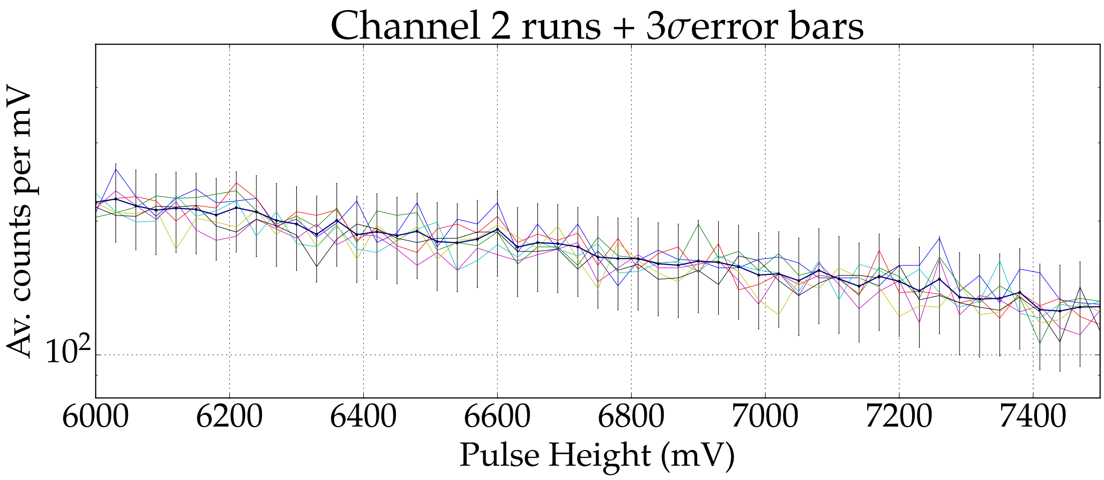
Channel 2 runs + 3σerror bars
Av. counts per mV
$10^2$
6000
6200
6400
6600
6800
7000
7200
7400
Pulse Height (mV)

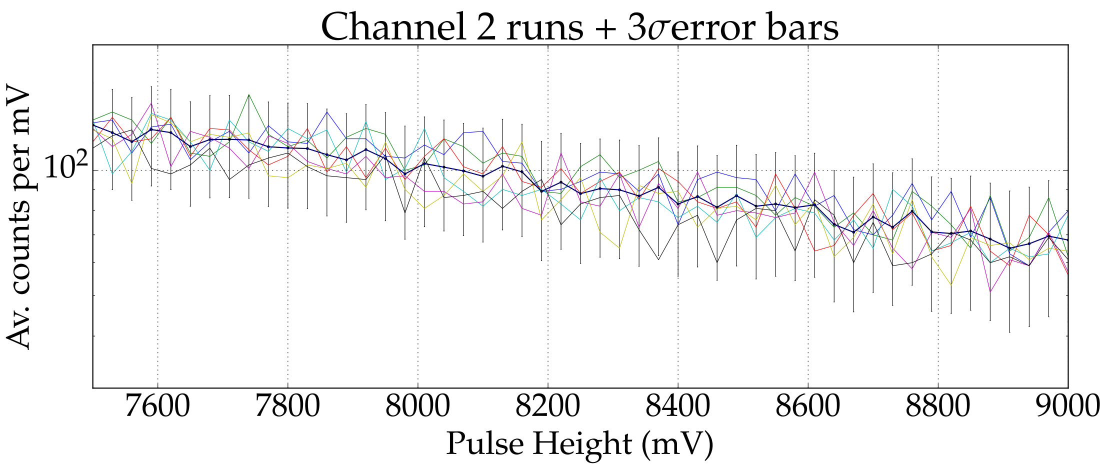
Channel 2 runs + 3σerror bars
Av. counts per mV
$10^2$
7600
7800
8000
8200
8400
8600
8800
9000
Pulse Height (mV)

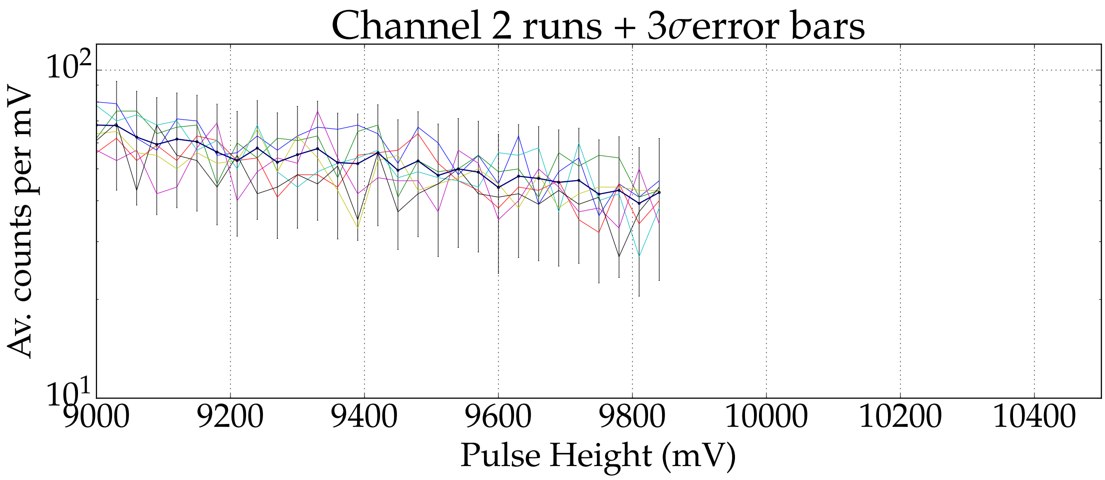


## B.3. Error analysis multichannel measurement

In the next 4 graphs, the $1\sigma$-error bars are shown for each of the 4 channels.

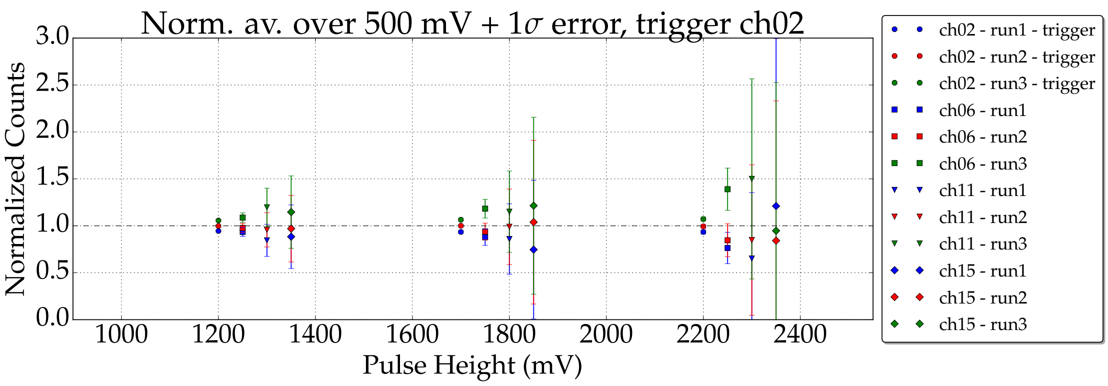


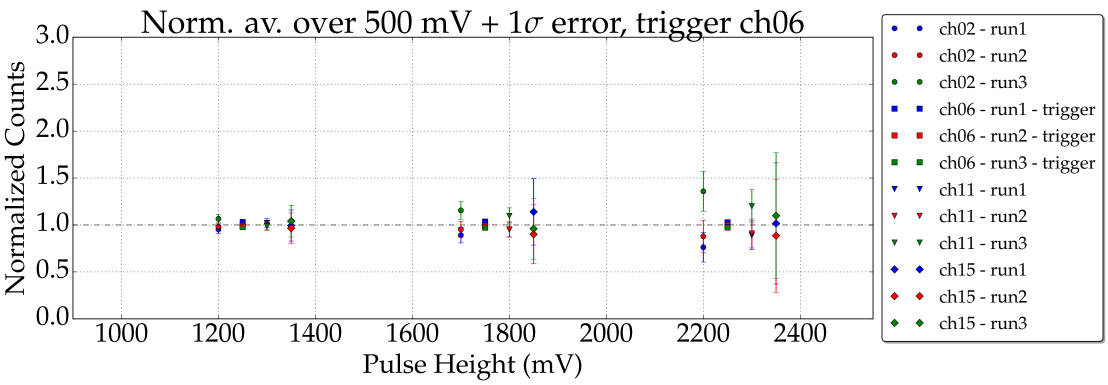

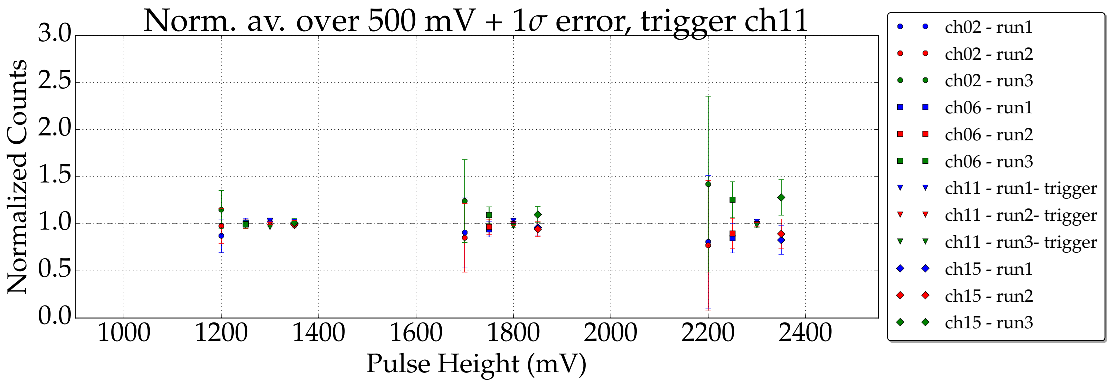
Norm. av. over 500 mV + 1σ error, trigger ch11
Normalized Counts
Pulse Height (mV)
0.0
0.5
1.0
1.5
2.0
2.5
3.0
1000
1200
1400
1600
1800
2000
2200
2400
ch02 - run1
ch02 - run2
ch02 - run3
ch06 - run1
ch06 - run2
ch06 - run3
ch11 - run1- trigger
ch11 - run2- trigger
ch11 - run3- trigger
ch15 - run1
ch15 - run2
ch15 - run3

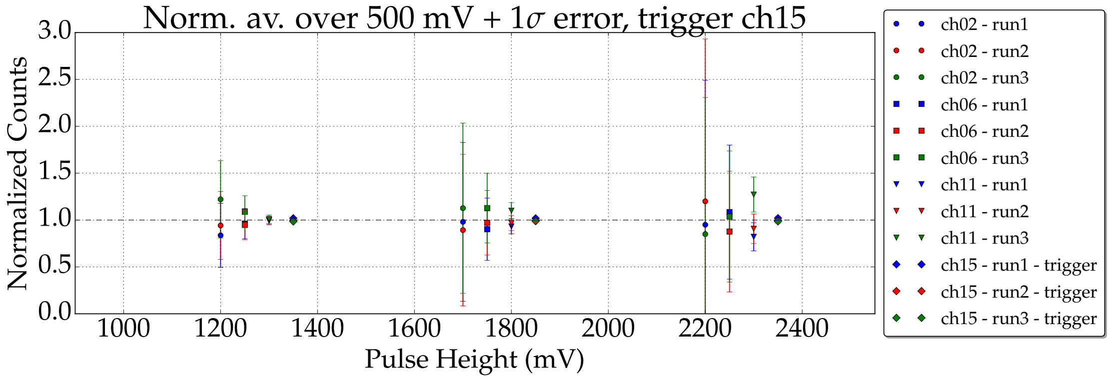
Norm. av. over 500 mV + 1σ error, trigger ch15
Normalized Counts
Pulse Height (mV)
0.0
0.5
1.0
1.5
2.0
2.5
3.0
1000
1200
1400
1600
1800
2000
2200
2400
ch02 - run1
ch02 - run2
ch02 - run3
ch06 - run1
ch06 - run2
ch06 - run3
ch11 - run1
ch11 - run2
ch11 - run3
ch15 - run1 - trigger
ch15 - run2 - trigger
ch15 - run3 - trigger

In the next 4 graphs, the $3\sigma$-error bars are shown for each of the 4 channels.

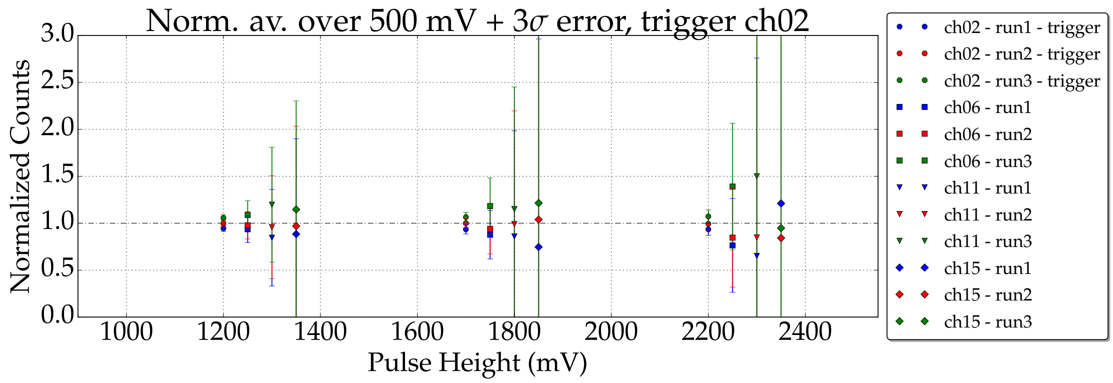


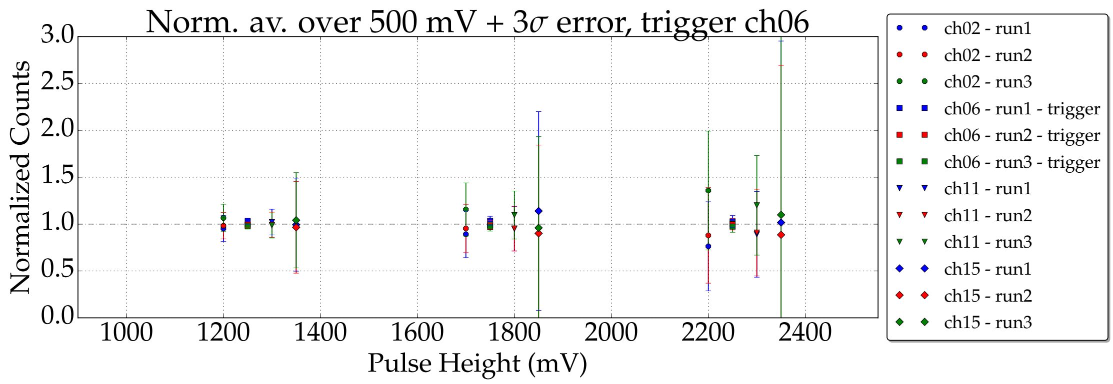


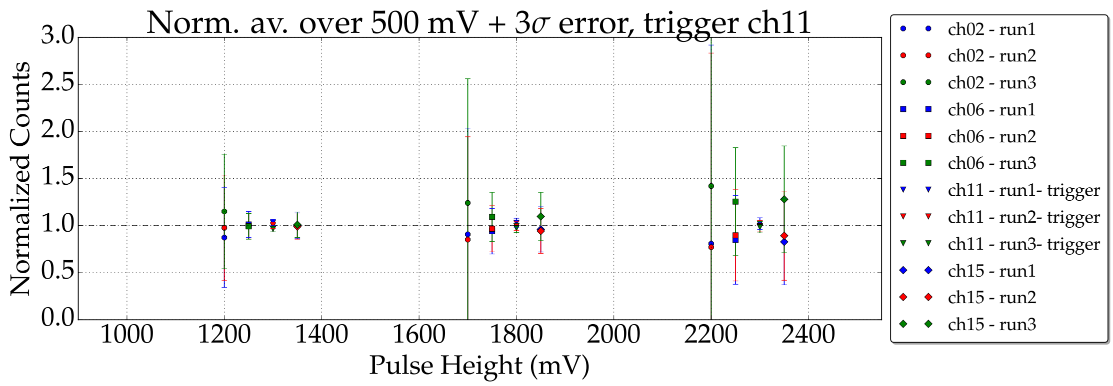

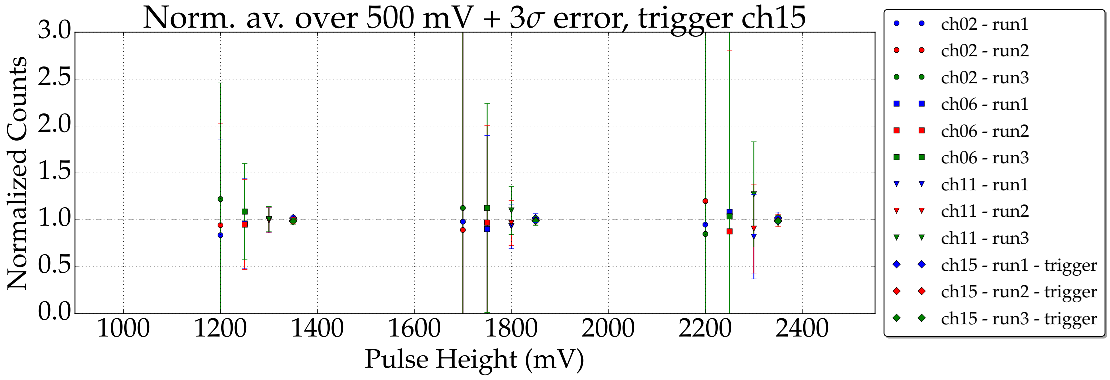
Norm. av. over 500 mV + 3σ error, trigger ch15
Normalized Counts
0.0
0.5
1.0
1.5
2.0
2.5
3.0
1000
1200
1400
1600
1800
2000
2200
2400
Pulse Height (mV)
ch02 - run1
ch02 - run2
ch02 - run3
ch06 - run1
ch06 - run2
ch06 - run3
ch11 - run1
ch11 - run2
ch11 - run3
ch15 - run1 - trigger
ch15 - run2 - trigger
ch15 - run3 - trigger

# C. Data pure gas measurements - Neon

In this appendix, all the data for neon-measurements in 3 different voltage-regions are shown. The first graph shows the result for a voltage of 192V/300V, the second graph for a voltage of 208V/400V and the last graph for a voltage of 225V/450V. In the first graph, however, only three out of the four channels are shown, since the last channel did not give any usable measurements because of trigger-issues.

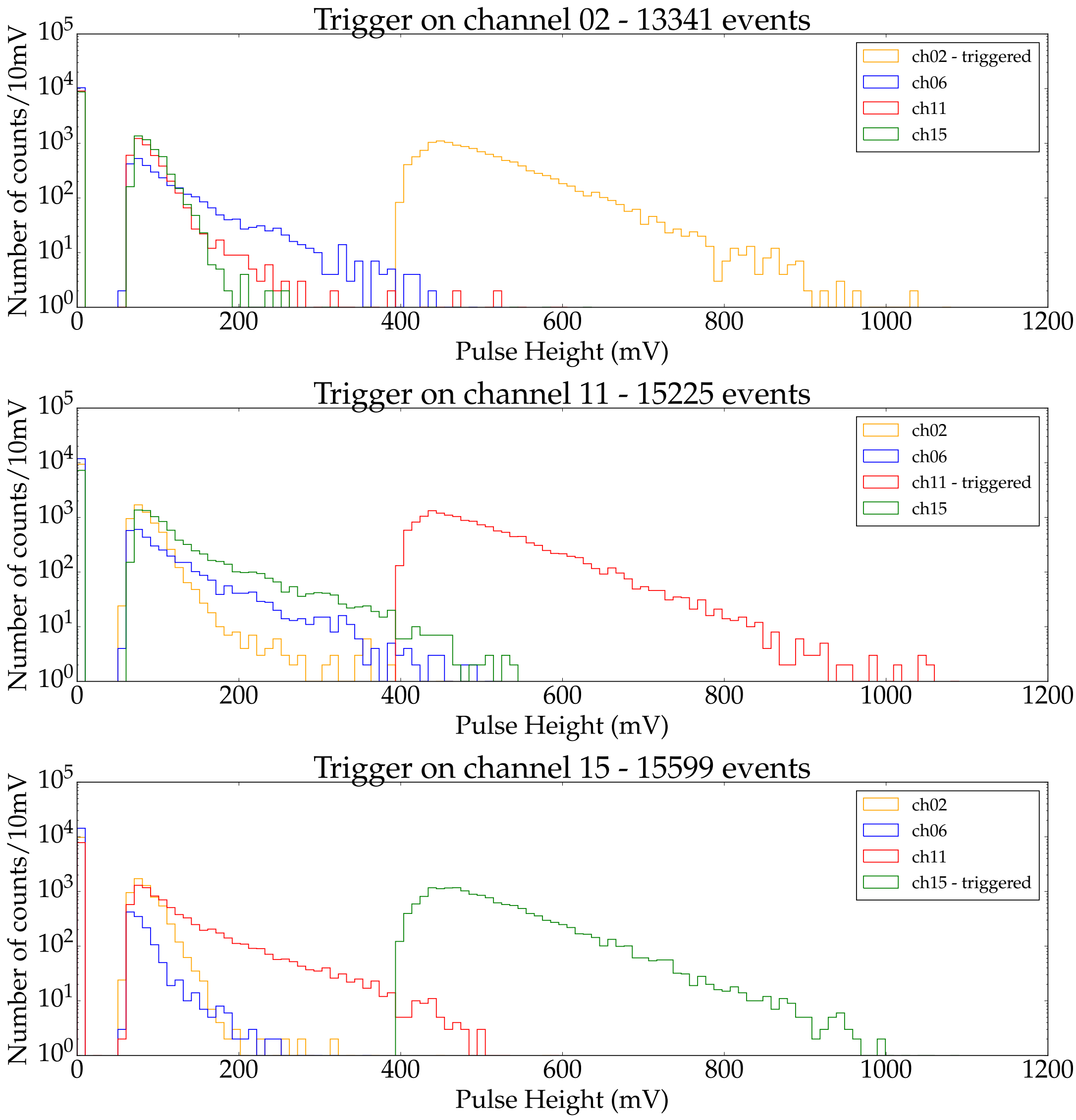


**Figure C.1.:** Neon Measurements at 192V/300V

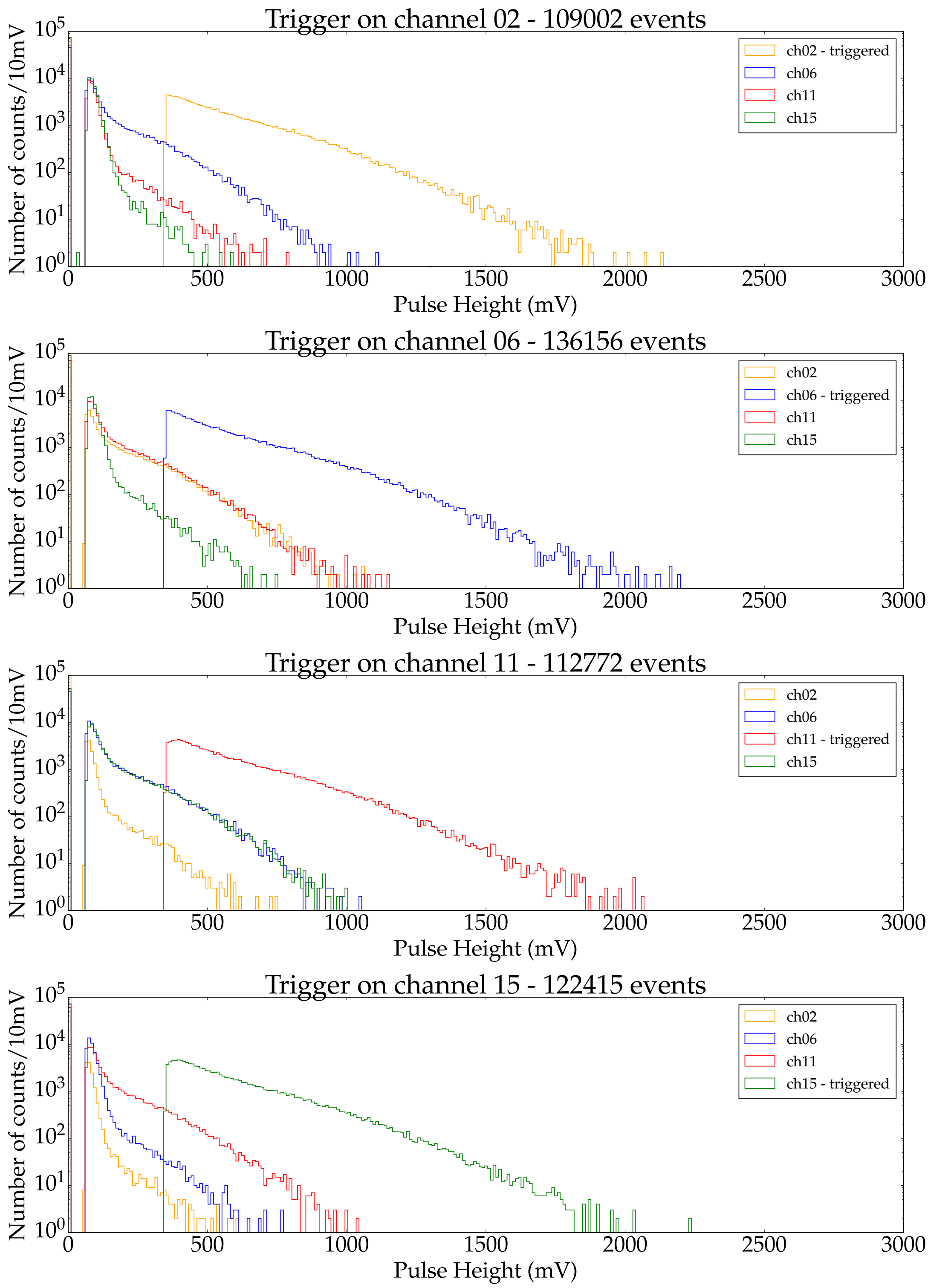


**Figure C.2.:** Neon Measurements at 208V/300V

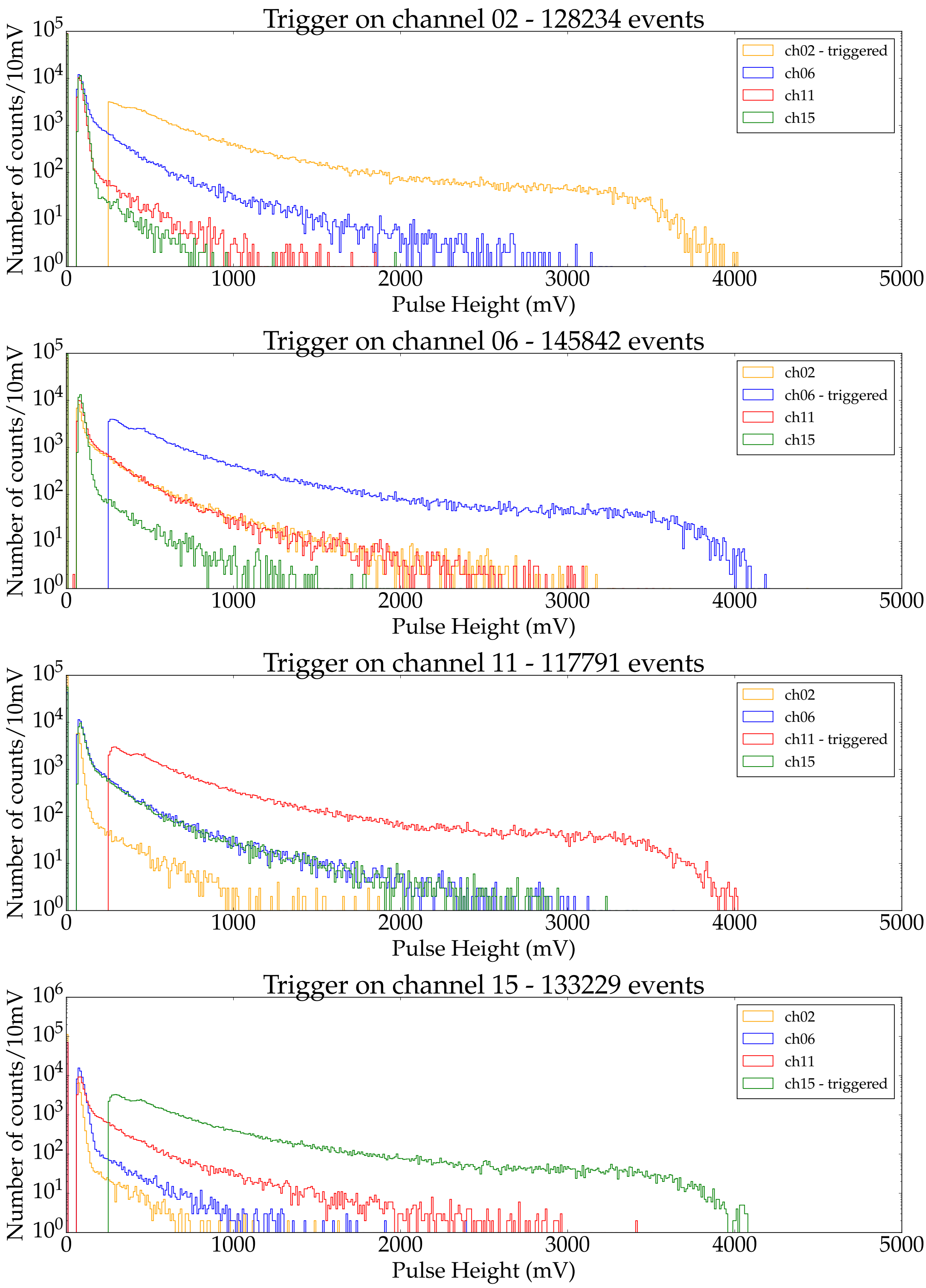


**Figure C.3.:** Neon Measurements at 225V/300V

# Bibliography

[1] M. Poli Lener, G. Corradi, C. Curceanu, D. Tagnani, A. Vidal, and J. Zmeskal, "Performances of an active target gem-based tpc for the amadeus experiment.," Modern Instrumentation, vol. 4, pp. 32–41, 2015.

[2] G. F. Knoll, Radiation Detection and Measurement. Wiley, 2010.

[3] "Cms physics technical design report volume i: Detector performance and software," tech. rep., CERN/LHCC, 2006.

[4] P. Gasik, "Development of gem-based read-out chambers for the upgrade of the alice tpc," Journal of Instrumentation, vol. 9, p. C04035, 2014.

[5] M. Adinolfi et al., "The {KLOE} drift chamber," Nuclear Instruments and Methods in Physics Research Section A: Accelerators, Spectrometers, Detectors and Associated Equipment, vol. 461, no. 1–3, pp. 25 – 28, 2001. 8th Pisa Meeting on Advanced Detectors.

[6] B. Ketzer, S. Bachmann, M. Capeans, M. Deutel, J. Friedrich, S. Kappler, I. Konorov, S. Paul, A. Placci, K. Reisinger, L. Ropelewski, L. Shekhtman, and F. Sauli, "Gem detectors for compass," Nuclear Science, IEEE Transactions on, vol. 48, pp. 1065–1069, Aug 2001.

[7] F. Sauli, "Gem: A new concept for electron amplification in gas detectors," Nuclear Instruments and Methods in Physics Research Section A: Accelerators, Spectrometers, Detectors and Associated Equipment, vol. 386, no. 2–3, pp. 531 – 534, 1997.

[8] F. Sauli, "Close view of a gem electrode." `http://gdd.web.cern.ch/GDD/`. Accessed: 2015-06-02.

[9] "Layout of a triple gem." `https://web2.infn.it/GEMINI/`. Accessed: 2015-06-03.

[10] U. Straumann and M. Ziegler, "Field configuration of a gem." `http://docs.exdat.com/docs/index-6761.html`. Accessed: 2015-06-03.

[11] "Working principle of a tpc." `https://panda-wiki.gsi.de/foswiki/bin/view/Tagpid/TpC`. Accessed: 2015-07-07.

# Curriculum Vitae

**Study**

| | |
|---|---|
| Apr 13 – Aug 15 | MSc in Physics, University of Vienna |
| July 12 - Aug 12 | Month-long internship at Stefan-Meyer-Institute for subatomic physics in Vienna, working for ASACUSA Experiment at CERN-AD |
| Sept 09 - Apr 13 | BSc in Physics, University of Vienna |

**Other activities**

| | |
|---|---|
| Nov 08 - Jul 09 | Temporary job at Fischer Gebäudetechnik AG in Neuenstadt am Kocher, Germany |
| Aug 08 - Sept 08 | Two-month trip through Europe |

**School**

| | |
|---|---|
| Sept 99 - Jun 08 | Eduard-Mörike-Gymnasium Neuenstadt am Kocher, Germany |
| Sept 95 - Jul 99 | Elementary school Langenbrettach, Germany |

Vienna, July 2015